*convertible*CAR-T cells provide a modular universal system for dose control of activity, flexible targeting, and versatile maintenance of CAR-cells

Kyle Landgraf, Steven R. Williams, Daniel Steiger, Dana Gebhart, Stephen Lok, David W. Martin, Kole T. Roybal, and Kaman Chan Kim*

* To whom correspondence should be addressed: kaman@xyphosinc.com

ABSTRACT

Current chimeric antigen receptor (CAR) cellular therapies, while remarkably efficacious, have a number of limitations that impact their efficacy, safety and perseverance in the clinical setting, including commitment to targeting a single antigen, utilization of non-human components, and lack of dose control. We have developed a universal CAR platform to function as a flexible and controllable system to address these limitations. An inert form of the NKG2D extracellular domain (iNKG2D) was used as the surface-exposed portion of the CAR and transduced into T cells to generate *convertible*CAR™-T cells. These cells were activated only when an immunological synapse was formed with a displayed antigenic target, mediated by a bispecific molecule comprised of an iNKG2D-exclusive orthogonal human ligand fused to an antigen-targeting antibody (MicAbody™). By altering the Fv domains of the MicAbody, cytolytic activity against a variety of antigen-expressing cell lines was demonstrated *in vitro*. In addition to sequential introduction of MicAbodies, arming *convertible*CAR-T cells with a combination of MicAbodies resulted in simultaneous activity against different antigen-containing targets. Additionally, activation and cytolytic functions of *convertible*CAR-T cells depended upon the dose of MicAbody introduced. Studies in NSG mice exploring efficacy against Raji tumors demonstrated dose-dependent control of tumor mass by rituximab-based MicAbody as well as by *convertible*CAR-T cells. We have also demonstrated that the exclusive ligand-receptor partnering enabled the targeted delivery of ligand-fused payloads to *convertible*CAR-T cells. Ligand fusion to CDC-enhanced Fc domains led to *in vitro* reduction of *convertible*CAR-T cells by human complement, thus offering the ability to reduce the levels of CAR cells in a patient without necessarily completely eliminating them. Selective delivery of a mutant IL-2 drove expansion of *convertible*CAR-T cells *in vitro* and promoted *in vivo* expansion and recovery. This ability to leverage the exclusive ligand-receptor interaction has profound implications for the ability to exogenously control *convertible*CAR-T cell expansion, persistence, and function within the patient. This, combined with the ability to switch targets and multiplex without modifying the CAR, enables the development of a highly modular and adaptable universal system to create a single autologous cell for all targets in a single donor patient or one allogeneic cell for all patients and all targets.

INTRODUCTION

The engineering of patient-derived T cells to express chimeric antigen receptors (CARs) has altered the landscape of adoptive cell therapies, providing scientists and clinicians the ability to harness the powerful cytolytic capabilities of T cells and direct them to specific antigen-expressing targets in an MHC-independent manner. Their initial application to treat refractory or relapsed hematologic malignancies has led to astounding response rates and inspired a surge of research interests and efforts to improve upon the original designs in order to strike the best balance of CAR-T cell potency, safety,

and persistence and drive their effective use in non-hematologic indications[1 2]. Current, second generation iterations of CAR-T cells utilize a single-chain variable fragment (scFv) from an antigen-specific antibody with or without a hinge domain, tethered to the cell via a transmembrane domain, which in turn is fused to one or more costimulatory domains (most commonly 4-1BB or CD28) along with CD3zeta[3 4]. Much of the initial optimization work has centered on identification of affinity-balanced targeting scFvs that minimally induce tonic signaling and exhaustion of CAR-T cells, optimizing hinge composition and length, combinatorial shuffling of costimulatory cassettes to augment T cell function, and exploring alternative means of genetically altering and expanding cells to reduce manufacturing times and promote the most desirable T cell subsets. Sufficient pre-clinical and clinical data have accumulated from the variations on prototype CAR architecture such that there is now a deeper appreciation of the subtleties that affect CAR-T function. However, target selection, indication, and even innate qualities of patient-donor T cells introduce significant variables that have precluded the generation of an archetypal CAR construct.

Pioneer CAR-T cell therapies are significantly inhibited by their utilization of a single-purpose targeting domain, lack of dose control, which contributes to cytokine release syndrome, and inability to address antigen loss which leads to disease relapse[5 6]. There is a need to develop a "universal" CAR-T cell system with expanded versatility such that it can be readily implemented for any and multiple targets and indications and that, ideally, would provide elements of dose control of activity expansion, and persistence - the combination of which have not been achieved with antigen-specific scFv-based CARs alone. Measures for added control of CAR-T cells that have been developed include suicide switches for elimination of CAR-Ts in clinical settings where life-threatening toxicities develop[7], CARs that can be induced by the addition of a small molecule[8], CAR expression that is induced by logic-gating systems to reduce on-target off-tumor toxicities[9], and even CAR-T cells engineered to secrete cytokines

---

[1] Carl H. June and Michel Sadelain, "Chimeric Antigen Receptor Therapy," *The New England Journal of Medicine* 379, no. 1 (05 2018): 64–73, https://doi.org/10.1056/NEJMra1706169.

[2] Julio C. Chavez and Frederick L. Locke, "CAR T Cell Therapy for B-Cell Lymphomas," *Best Practice & Research. Clinical Haematology* 31, no. 2 (June 2018): 135–46, https://doi.org/10.1016/j.beha.2018.04.001.

[3] "Programming CAR-T Cells to Kill Cancer | Nature Biomedical Engineering," accessed August 28, 2018, https://www.nature.com/articles/s41551-018-0235-9.

[4] Wendell A. Lim and Carl H. June, "The Principles of Engineering Immune Cells to Treat Cancer," *Cell* 168, no. 4 (09 2017): 724–40, https://doi.org/10.1016/j.cell.2017.01.016.

[5] Jae H. Park et al., "Long-Term Follow-up of CD19 CAR Therapy in Acute Lymphoblastic Leukemia," *The New England Journal of Medicine* 378, no. 5 (01 2018): 449–59, https://doi.org/10.1056/NEJMoa1709919.

[6] Elena Sotillo et al., "Convergence of Acquired Mutations and Alternative Splicing of CD19 Enables Resistance to CART-19 Immunotherapy," *Cancer Discovery* 5, no. 12 (December 2015): 1282–95, https://doi.org/10.1158/2159-8290.CD-15-1020.

[7] Iulia Diaconu et al., "Inducible Caspase-9 Selectively Modulates the Toxicities of CD19-Specific Chimeric Antigen Receptor-Modified T Cells," *Molecular Therapy: The Journal of the American Society of Gene Therapy* 25, no. 3 (01 2017): 580–92, https://doi.org/10.1016/j.ymthe.2017.01.011.

[8] Reona Sakemura et al., "A Tet-On Inducible System for Controlling CD19-Chimeric Antigen Receptor Expression upon Drug Administration," *Cancer Immunology Research* 4, no. 8 (2016): 658–68, https://doi.org/10.1158/2326-6066.CIR-16-0043.

[9] Kole T. Roybal et al., "Precision Tumor Recognition by T Cells With Combinatorial Antigen-Sensing Circuits," *Cell* 164, no. 4 (February 11, 2016): 770–79, https://doi.org/10.1016/j.cell.2016.01.011.

to promote expansion or enhance solid tumor efficacy[10 11 12 13]. To address antigen loss, dual targeting by linked, tandem scFvs recognizing distinct antigens have demonstrated efficacy but can be challenging to optimize and do not inherently promote CAR versatility[14 15 16 17]. There have also been several strategies (termed "switch", "adaptor", or "universal immune receptors") developed where the extracellular component of the CAR construct is agnostic to the antigen with targeting activated by a bifunctional adaptor molecule that bridges the extracellular portion of the CAR to an antigen in order to generate an immunological synapse (reviewed in[18]). These include a CAR comprised of CD16a (FcγRIIIa), thus allowing the use of approved therapeutic monoclonal antibodies to direct the CAR cell to a targeted cell to induce ADCC [19]; CARs that have scFvs recognizing short peptides or a fluorophore which are then attached to an antigen-targeting moiety[2021 22]; and a split leucine zipper system in which one part of the zipper functions as the CAR extracellular domain and the other cognate zipper part is tethered to a tumor-targeting scFv[23]. There are also CAR concepts in development to address the hurdles in the solid tumor environment by blocking or even converting suppressive signals into activating ones or that allow

---

[10] Kole T. Roybal et al., "Engineering T Cells with Customized Therapeutic Response Programs Using Synthetic Notch Receptors," *Cell* 167, no. 2 (October 6, 2016): 419-432.e16, https://doi.org/10.1016/j.cell.2016.09.011.
[11] Lenka V. Hurton et al., "Tethered IL-15 Augments Antitumor Activity and Promotes a Stem-Cell Memory Subset in Tumor-Specific T Cells," *Proceedings of the National Academy of Sciences of the United States of America* 113, no. 48 (29 2016): E7788–97, https://doi.org/10.1073/pnas.1610544113.
[12] Markus Chmielewski et al., "IL-12 Release by Engineered T Cells Expressing Chimeric Antigen Receptors Can Effectively Muster an Antigen-Independent Macrophage Response on Tumor Cells That Have Shut down Tumor Antigen Expression," *Cancer Research* 71, no. 17 (September 1, 2011): 12, https://doi.org/10.1158/0008-5472.CAN-11-0103.
[13] Ling Zhang et al., "Improving Adoptive T Cell Therapy by Targeting and Controlling IL-12 Expression to the Tumor Environment," *Molecular Therapy: The Journal of the American Society of Gene Therapy* 19, no. 4 (April 2011): 751–59, https://doi.org/10.1038/mt.2010.313.
[14] Marco Ruella et al., "Dual CD19 and CD123 Targeting Prevents Antigen-Loss Relapses after CD19-Directed Immunotherapies," *The Journal of Clinical Investigation* 126, no. 10 (October 3, 2016): 3814–26, https://doi.org/10.1172/JCI87366.
[15] Terry J. Fry et al., "CD22-Targeted CAR T Cells Induce Remission in B-ALL That Is Naive or Resistant to CD19-Targeted CAR Immunotherapy," *Nature Medicine* 24, no. 1 (January 2018): 22, https://doi.org/10.1038/nm.4441.
[16] Dina Schneider et al., "A Tandem CD19/CD20 CAR Lentiviral Vector Drives on-Target and off-Target Antigen Modulation in Leukemia Cell Lines," *Journal for Immunotherapy of Cancer* 5 (2017): 42, https://doi.org/10.1186/s40425-017-0246-1.
[17] Meenakshi Hegde et al., "Tandem CAR T Cells Targeting HER2 and IL13Rα2 Mitigate Tumor Antigen Escape," *The Journal of Clinical Investigation* 126, no. 8 (01 2016): 3036–52, https://doi.org/10.1172/JCI83416.
[18] Nicholas G. Minutolo, Erin E. Hollander, and Daniel J. Powell, "The Emergence of Universal Immune Receptor T Cell Therapy for Cancer," *Frontiers in Oncology* 9 (2019): 176, https://doi.org/10.3389/fonc.2019.00176.
[19] Ko Kudo et al., "T Lymphocytes Expressing a CD16 Signaling Receptor Exert Antibody-Dependent Cancer Cell Killing," *Cancer Research* 74, no. 1 (January 1, 2014): 93–103, https://doi.org/10.1158/0008-5472.CAN-13-1365.
[20] Jennifer S. Y. Ma et al., "Versatile Strategy for Controlling the Specificity and Activity of Engineered T Cells," *Proceedings of the National Academy of Sciences of the United States of America* 113, no. 4 (January 26, 2016): E450-458, https://doi.org/10.1073/pnas.1524193113.
[21] M. Cartellieri et al., "Switching CAR T Cells on and off: A Novel Modular Platform for Retargeting of T Cells to AML Blasts," *Blood Cancer Journal* 6, no. 8 (12 2016): e458, https://doi.org/10.1038/bcj.2016.61.
[22] David T. Rodgers et al., "Switch-Mediated Activation and Retargeting of CAR-T Cells for B-Cell Malignancies," *Proceedings of the National Academy of Sciences of the United States of America* 113, no. 4 (January 26, 2016): E459-468, https://doi.org/10.1073/pnas.1524155113.
[23] Jang Hwan Cho, James J. Collins, and Wilson W. Wong, "Universal Chimeric Antigen Receptors for Multiplexed and Logical Control of T Cell Responses," *Cell* 173, no. 6 (May 31, 2018): 1426-1438.e11, https://doi.org/10.1016/j.cell.2018.03.038.

localized secretion of checkpoint blocking scFvs by the CAR-T cell[24 25]. However, there is no single receptor system that can be modulated extracellularly and has been demonstrated to have the potential for all the following: (1) targeting flexibility to direct T cell activity to any antigen of choice, (2) multiplex capabilities to reduce the potential for antigen-loss related relapse, (3) dose control for differential engagement of CAR-T cells, and (4) selective delivery of extracellular reagents to CAR-expressing cells to functionally modulate them (e.g. ablate or promote their expansion, affect differentiation).

NKG2D is an activating receptor expressed as a type II homodimeric integral protein on the surface of Natural Killer (NK) cells, some myeloid cells and certain T cells[26 27 28]. Human NKG2D has eight distinct natural MIC ligands (MICA, MICB, ULBP1 through ULBP6) that are upregulated on the surface of cells in response to a variety of stresses, damage, or cellular transformation[29 30 31]. The differential regulation of NKG2D ligands, such as the polymorphic MICA and MICB, is important for providing the immune system with a means to identify and respond to a broad range of emergency cues while still protecting healthy cells from unwanted attack[32 33]. Viral infection is a common inducer of MIC ligand expression and identifies the viral-infected cell for NK- or T cell-mediated containment[34 35]. Expression of MIC proteins is also induced on many tumor cells where their presence can render them sensitive to targeting and lysis by NK cells[36 37]. The structure of NKG2D ectodomain, several soluble ligands, and the bound complex of ligands to the ectodomain have been solved, revealing a saddle-like groove in the homodimer interface which engages the α1-α2 domains of ligands. The ability of NKG2D to bind very disparate ligands with their respective α1-α2 domains ranging from 20-96% identity can be explained by

---

[24] Benjamin Boyerinas et al., "Abstract 602: A Novel TGF-β/IL-12R Signal Conversion Platform That Protects CAR T Cells from TGF-β-Mediated Immune Suppression and Concurrently Amplifies Effector Function," *Cancer Research* 77, no. 13 Supplement (July 1, 2017): 602–602, https://doi.org/10.1158/1538-7445.AM2017-602.

[25] Sarwish Rafiq et al., "Targeted Delivery of a PD-1-Blocking ScFv by CAR-T Cells Enhances Anti-Tumor Efficacy in Vivo," *Nature Biotechnology*, August 13, 2018, https://doi.org/10.1038/nbt.4195.

[26] Lewis L. Lanier, "NK CELL RECEPTORS," *Annual Review of Immunology* 16, no. 1 (April 1998): 359–93, https://doi.org/10.1146/annurev.immunol.16.1.359.

[27] J. P. Houchins et al., "DNA Sequence Analysis of NKG2, a Family of Related CDNA Clones Encoding Type II Integral Membrane Proteins on Human Natural Killer Cells," *The Journal of Experimental Medicine* 173, no. 4 (April 1, 1991): 1017–20.

[28] S. Bauer et al., "Activation of NK Cells and T Cells by NKG2D, a Receptor for Stress-Inducible MICA," *Science (New York, N.Y.)* 285, no. 5428 (July 30, 1999): 727–29.

[29] V. Groh et al., "Cell Stress-Regulated Human Major Histocompatibility Complex Class I Gene Expressed in Gastrointestinal Epithelium," *Proceedings of the National Academy of Sciences of the United States of America* 93, no. 22 (October 29, 1996): 12445–50.

[30] V. Groh et al., "Recognition of Stress-Induced MHC Molecules by Intestinal Epithelial Gammadelta T Cells," *Science (New York, N.Y.)* 279, no. 5357 (March 13, 1998): 1737–40.

[31] N. W. Zwirner, K. Dole, and P. Stastny, "Differential Surface Expression of MICA by Endothelial Cells, Fibroblasts, Keratinocytes, and Monocytes," *Human Immunology* 60, no. 4 (April 1999): 323–30.

[32] H. A. Stephens, "MICA and MICB Genes: Can the Enigma of Their Polymorphism Be Resolved?," *Trends in Immunology* 22, no. 7 (July 2001): 378–85.

[33] Thomas Spies, "Regulation of NKG2D Ligands: A Purposeful but Delicate Affair," *Nature Immunology* 9, no. 9 (September 2008): 1013–15, https://doi.org/10.1038/ni0908-1013.

[34] Groh et al., "Recognition of Stress-Induced MHC Molecules by Intestinal Epithelial Gammadelta T Cells."

[35] A. Cerwenka and L. L. Lanier, "Natural Killer Cells, Viruses and Cancer," *Nature Reviews. Immunology* 1, no. 1 (October 2001): 41–49, https://doi.org/10.1038/35095564.

[36] Andreas Busche et al., "Natural Killer Cell-Mediated Rejection of Experimental Human Lung Cancer by Genetic Overexpression of Major Histocompatibility Complex Class I Chain-Related Gene A," *Human Gene Therapy* 17, no. 2 (February 2006): 135–46, https://doi.org/10.1089/hum.2006.17.135.

[37] Maelig G. Morvan and Lewis L. Lanier, "NK Cells and Cancer: You Can Teach Innate Cells New Tricks," *Nature Reviews. Cancer* 16, no. 1 (January 2016): 7–19, https://doi.org/10.1038/nrc.2015.5.

the observation that they adopt a very similar structure[38 39 40 41 42]. Based upon the available structure-function information for NKG2D-MIC binding (Protein Data Bank accession codes 1HYR, 4SOU), we have engineered a novel and exclusive receptor-ligand interaction to generate the components for our *convertible*CAR™ system. NKG2D was mutated to render it incapable of engaging any natural ligands[43], and orthogonal ligand variants that selectively engaged with the inert NKG2D (iNKG2D) and not the wild-type receptor were generated. The iNKG2D serves as the extracellular component of our CAR construct while the orthogonal U2S3 α1-α2 domain variant is expressed as a fusion to antigen-specific antibodies, generating bispecifics termed MicAbodies™. MicAbodies are capable of directing and activating iNKG2D-CAR expressing T cells when the appropriate antigen is displayed in a two-dimensional format. Keeping the iNKG2D-CAR receptor constant, we have demonstrated that T cells can be differentially targeted to different tumor cells by sequentially altering or even multiplexing the introduced MicAbody to target multiple antigens simultaneously. In a disseminated *in vivo* Raji tumor model, efficacy required both the iNKG2D-CAR and MicAbody and demonstrated a dose-related response that depended on both the administered dose of MicAbody and of iNKG2D-CAR T cells. Lastly, we have determined that U2S3 can be used as a means of addressing molecules for targeted delivery to iNKG2D-expressing cells and that we can use this privileged partnering to specifically target the *convertible*CAR cells for complement-mediated killing or drive their expansion *in vitro* and *in vivo* with a fusion to a mutant cytokine, e.g. IL-2. This highly modular *convertible*CAR system leverages the significant body of information behind antibody discovery, development, and manufacturing and nimbly integrates it with the tremendous potential of adoptive cell therapies.

MATERIALS AND METHODS

Protein cloning, expression, and purification. The wild-type ectodomain of NKG2D (UniProtKB P26718, residues 78-216; https://www.uniprot.org) was expressed as a fusion to the C-terminus of human IgG1 Fc via a short factor Xa recognizable Ile-Glu-Gly-Arg linker (Fc-wtNKG2D). Inert NKG2D variants comprising either a single Y152A (iNKG2D.YA) or double Y152A/Y199A substitution (iNKG2D.AF) at the key tyrosine residues critical for MIC ligand interaction[44] were generated by PCR-mediated mutagenesis or synthesized (gBlocks®, Integrated DNA Technologies). DNA constructs for Fc-NKG2D molecules were expressed in Expi293™ cells (Thermo Fisher Scientific) and dimeric secreted protein purified by Protein A affinity chromatography (Pierce™ #20334, Thermo Fisher). Eluted material was characterized and further purified by size-exclusion chromatography (SEC) on an ÄKTA Pure system

---

[38] P. Li et al., "Complex Structure of the Activating Immunoreceptor NKG2D and Its MHC Class I-like Ligand MICA," *Nature Immunology* 2, no. 5 (May 2001): 443–51, https://doi.org/10.1038/87757.

[39] S. Radaev et al., "Conformational Plasticity Revealed by the Cocrystal Structure of NKG2D and Its Class I MHC-like Ligand ULBP3," *Immunity* 15, no. 6 (December 2001): 1039–49.

[40] Jianmin Zuo et al., "A Disease-Linked ULBP6 Polymorphism Inhibits NKG2D-Mediated Target Cell Killing by Enhancing the Stability of NKG2D Ligand Binding," *Science Signaling* 10, no. 481 (May 30, 2017), https://doi.org/10.1126/scisignal.aai8904.

[41] Benjamin J. McFarland and Roland K. Strong, "Thermodynamic Analysis of Degenerate Recognition by the NKG2D Immunoreceptor: Not Induced Fit but Rigid Adaptation," *Immunity* 19, no. 6 (December 2003): 803–12.

[42] Steffen Müller et al., "Structure of the HCMV UL16-MICB Complex Elucidates Select Binding of a Viral Immunoevasin to Diverse NKG2D Ligands," *PLoS Pathogens* 6, no. 1 (January 15, 2010): e1000723, https://doi.org/10.1371/journal.ppat.1000723.

[43] David J. Culpepper et al., "Systematic Mutation and Thermodynamic Analysis of Central Tyrosine Pairs in Polyspecific NKG2D Receptor Interactions," *Molecular Immunology* 48, no. 4 (January 2011): 516–23, https://doi.org/10.1016/j.molimm.2010.10.007.

[44] Culpepper et al.

using Superdex 200 columns (GE Life Sciences). Correctly assembled, size-appropriate monomeric material was fractionated into phosphate-buffered saline (PBS).

The α_1-α_2 domains of human MICA*001 (UniProtKB Q29983, residues 24-205), MICB (UniProtKB Q29980.1, residues 24-205), ULBP1 (UniProtKB Q9BZM6, residues 29-212), ULBP2 (UniProtKB Q9BZM5, residues 29-212), ULBP3 (UniProtKB Q9BZM4, 30-212), ULBP5 (NCBI accession NP_001001788.2, residues 29-212), ULBP6 (UniProtKB, residue 29-212) were cloned with a C-terminal 6x-His tag, monomeric protein was purified from Expi293™ supernatants Ni-NTA resin (HisPur™, Thermo Fisher), and eluted material exchanged into PBS with Sephadex G-25 in PD-10 Desalting Columns (GE Healthcare Life Sciences).

MIC ligands and orthogonal variants were cloned by ligation-independent assembly (HiFi DNA Assembly Master Mix, NEB #E2621) as fusions to the C-terminus of either the kappa light-chain or the heavy-chain of human IgG1 antibodies via either an APTSSSGGGGS or GGGS linker, respectively. Additionally, D265A/N297A (Kabat numbering) mutations were introduced into the CH2 domain of the heavy chain of all antibody and MicAbody clones to reduce binding to all FcγR receptors thus eliminating antibody-dependent cell cytotoxicity (ADCC) function[45]. Heavy- and light-chain plasmid DNAs (in the mammalian expression vector pD2610-V12 (ATUM) for a given antibody clone were co-transfected into Expi293™ cells and purified by Protein A resin. Monoclonal antibodies for which fusions were generated include anti-CD20 clone rituximab, anti-Her2 clone trastuzumab, and anti-FGFR3 antibody clone R3Mab[46] and were all generated by substituting with the appropriate VL or VH domain into either the kappa light-chain or ADCC- IgG1 heavy-chain. For any monoclonal antibody fusion generated, the two copies of ligand were present on either the heavy chain or light chain, thus creating a bispecific molecule termed a MicAbody™.

Engineering of inert NKG2D, identification of orthogonal ligand variants, and MicAbody characterization. Bio-layer interferometry (BLI) with the FortéBio Octet system (Pall FortéBio LLC) was implemented to validate loss of wild-type MIC ligand binding by iNKG2D. Fc-wtNKG2D or Fc-iNKG2D.YA was captured on anti-human IgG Fc capture (AHC) biosensor tips. After baseline establishment, tips were exposed to a titration series of monomeric MIC-His ligands and association/dissociation kinetics monitored. Additionally, ELISA (enzyme-linked immunosorbent assay) binding assays were performed with MICA-Fc, MICB-Fc, ULBP1-Fc, ULBP2-Fc, ULBP3-Fc, or ULBP4-Fc (R&D Systems) coated onto microtiter plates, a titration of biotinylated Fc-wtNKG2D or Fc-iNKG2D.YA, detected with streptavidin-HRP (R&D Systems #DY998), and developed with 1-Step Ultra TMB ELISA (Thermo Fisher #34208). Similar experiments were performed with the iNKG2D.AF inert variant by comparing wild-type ligand binding to Fc-wtNKG2D and Fc-iNKG2D.AF.

Phage display was employed to engineer orthogonal ULBP2 α1-α2 variants that exhibited selective binding to either iNKG2D.YA or iNKG2D.AF and greatly diminished engagement with wtNKG2D. Synthetic DNA libraries were generated for the α1-α2 domain of ULBP2 where codons of helix 2 (residues 74-78, numbering based upon mature protein) or helix 4 (residues 156-160) that in the bound state are positioned in close proximity to the Y152 positions on the natural NKG2D receptor[47] were

---

[45] R. L. Shields et al., "High Resolution Mapping of the Binding Site on Human IgG1 for Fc Gamma RI, Fc Gamma RII, Fc Gamma RIII, and FcRn and Design of IgG1 Variants with Improved Binding to the Fc Gamma R," *The Journal of Biological Chemistry* 276, no. 9 (March 2, 2001): 6591–6604, https://doi.org/10.1074/jbc.M009483200.

[46] Jing Qing et al., "Antibody-Based Targeting of FGFR3 in Bladder Carcinoma and t(4;14)-Positive Multiple Myeloma in Mice," *The Journal of Clinical Investigation* 119, no. 5 (May 2009): 1216–29, https://doi.org/10.1172/JCI38017.

[47] Müller et al., "Structure of the HCMV UL16-MICB Complex Elucidates Select Binding of a Viral Immunoevasin to Diverse NKG2D Ligands."

replaced with NNK [FIGURE 1A and 1B]. Additionally, R81W was incorporated since helix 4 libraries could not be generated without it, suggesting a compensatory stabilizing role. Libraries exploring helix 2 alone, helix 4 alone, or the combination were cloned as fusions to the pIII minor coat protein of M13 phage, and phage particles displaying the mutagenized α1-α2 domain variants were produced in SS320 *E.coli* cells according to standard methods[48] [49]. These α1-α2 phage display libraries were selected for high binding affinity to either inert NKG2D.YA variant by capturing phage clones with either biotinylated Fc-iNKG2D.YA or Fc-iNKG2D.AF protein (EZ-Link™ NHS-Biotin Kit, Thermo Fisher #20217) and enriching by cycling through four rounds of competitive selection with increasing concentrations of non-biotinylated Fc-wtNKG2D. Positive phage clones were verified for preferential binding to plate-bound Fc-iNKG2D.YA or Fc-iNKG2D.AF versus Fc-wtNKG2D by spot ELISA and bound phage detected with biotinylated M13 phage coat protein monoclonal antibody E1 (Thermo Fisher # MA1-34468) followed by incubation with streptavidin-HRP. Variants were sequenced then cloned as human IgG1 monoclonal antibody fusions (see above).

To confirm that selectivity of orthogonal variants was maintained in the bivalent MicAbody format, ELISAs comparing binding to Fc-wtNKG2D with Fc-iNKG2D.YA or Fc-iNKG2D.AF coated wells were performed with MicAbody binding detected using an HRP-conjugated mouse-anti-human kappa chain antibody (Abcam #ab79115). Affinity of both monomeric and antibody-fused ULBP2 variants was also determined by Octet analysis as described above. Additionally, thermal stability assays were performed with rituximab parent (ADCC-) and both heavy- and light-chain fusions of Rituximab-U2S3. Equal amounts of protein were subject to a +1°C/minute melting curve in the presence of SYPRO Orange (Millipore Sigma #S5692), changes in fluorescence quantified in a StepOnePlus™ Real-Time PCR System (Thermo Fisher), and fluorescence profiles overlayed.

CAR construction, lentiviral production, human primary T cell isolation, and lentiviral transduction. Human-codon optimized DNA (Invitrogen GeneArt Gene Synthesis, Thermo Fisher) comprising the CD8α-chain signal sequence, NKG2D variant, CD8α hinge and transmembrane domains, 4-1BB, CD3ζ, and eGFP were cloned into the pHR-PGK transfer plasmid[50] for second generation Pantropic VSV-G pseudotyped lentivirus production along with packaging plasmids pCMVdR8.91 and pMD2.G. The VH and VL domains of rituximab separated by a $(GGGGS)_3$ linker were substituted for the NKG2D module to generate the rituximab scFv-based CAR (RITscFv-CAR). For each batch of lentivirus produced, $6x10^6$ Lenti-X 293T (Takara Bio #632180) cells were seeded in a 10 cm dish the day prior to transfection. Then 12.9 µg pCMVdR8.91, 2.5 µg pMD2.G and 7.2 µg of the pHR-PGK-CAR constructs were combined in 720 µl Opti-MEM™ (Thermo Fisher # 31985062) then mixed with 67.5 µl of Fugene HD (Promega Corp. #E2311), briefly vortexed, and incubated at room temperature for 10 minutes before adding to the dish of cells. After two days, supernatants were collected by centrifugation and passed through 0.22 µm filters. Five-times concentrated PEG-6000 and NaCl were added to achieve final concentrations of 8.5% PEG-6000 (Hampton Research #HR2-533) and 0.3 M NaCl, incubated on ice for two hours, then centrifuged at 3500 rpm at 4°C for 20 minutes. Concentrated viral particles were resuspended in 0.01 volume of PBS, and stored frozen at -80°C.

---

[48] Raffi Tonikian et al., "Identifying Specificity Profiles for Peptide Recognition Modules from Phage-Displayed Peptide Libraries," *Nature Protocols* 2, no. 6 (2007): 1368–86, https://doi.org/10.1038/nprot.2007.151.

[49] Jennifer Andris-Widhopf et al., "Generation of Human ScFv Antibody Libraries: PCR Amplification and Assembly of Light- and Heavy-Chain Coding Sequences," *Cold Spring Harbor Protocols* 2011, no. 9 (September 1, 2011), https://doi.org/10.1101/pdb.prot065573.

[50] Leonardo Morsut et al., "Engineering Customized Cell Sensing and Response Behaviors Using Synthetic Notch Receptors," *Cell* 164, no. 4 (February 11, 2016): 780–91, https://doi.org/10.1016/j.cell.2016.01.012.

For primary human T cell isolation, a Human Peripheral Blood Leuko Pak (STEMCELL Technologies #70500.1) from an anonymous donor was diluted with an equivalent volume of PBS + 2% FBS, then centrifuged at 500 x g for 10 minutes at room temperature. Cells were resuspended at $5x10^7$ cells/ml in PBS + 2% FBS and CD4+ or CD8+ cells enriched by negative selection with the RosetteSEP™ system (#15062 for CD4 and #15023 for CD8, STEMCELL Tech.) by addition of 50 µl of isolation cocktail per ml of cells and incubating for five minutes at room temperature. Subsequently, 50 µl of RapidSpheres™ (STEMCELL Tech EasySep™ Human CD4 T Cell Isolation Kit #17952 or EasySep Human CD8 T Cell Isolation Kit #17953) were added per ml of cells and PBS buffer added to top up the sample (to 25 ml for samples ≤20 ml or to 50 ml for samples >20 ml). Cells were isolated for 10 minutes with an EasySEP™ magnet (STEMCELL) followed by removal of buffer while maintaining the magnetic field. Enriched cells were transferred into new tubes with fresh buffer and the magnet reapplied for a second round of enrichment after which cells were resuspended, counted, and cryopreserved at $10\text{-}15x10^6$ cells/cryovial in RPMI-1640 (Corning Inc. #15-040-CV), 20% human AB serum (Valley Biomedical #HP1022), 10% DMSO (Alfa Aesar #42780).

For lentiviral transduction, one vial of cryopreserved cells was thawed and added to 10 ml T cell medium (X-Vivo 15 media, Lonza #04-418Q; 5% human AB serum; 10 mM neutralized N-acetyl-L-Cysteine, Sigma-Aldrich #A9165 ; 1X 2-mercaptoethanol; 30 IUe/ml Peprotech recombinant human IL-2 "rhIL-2" #200-02). Cells were centrifuged at 400 x g for 5 minutes then resuspended in 10 ml T cell medium and adjusted to $1x10^6$/ml and plated at 1 ml/well in a 24 well plate. After an overnight rest 20 uL of Dynabeads™ Human T-Activator CD3/CD28 (Thermo Fisher #1131D) were added per well and incubated for 24 hours. Concentrated lentiviral particles (50 µL) were added per well, cells incubated overnight, then transferred to T25 flasks with an added 6 ml T-cell medium. After three days of expansion, Dynabeads were removed, transduction efficiency assessed by flow cytometry, back-diluted to $5x10^5$ cells/mL, and cell density monitored daily to ensure they did not exceed $4x10^6$ cells/ml. When necessary, surface expression of iNKG2D was correlated with GFP expression using a MicAbody and detecting with PE-anti-human kappa chain (Abcam #ab79113) or by directly conjugating the Rituximab-MicAbody to Alexa Fluor 647 (Alexa Fluor Protein Labeling Kit #A20173, Thermo Fisher). The amount of iNKG2D expression on the surface of *convertible*CAR-CD8 cells was quantified using Alexa Fluor 647 conjugated Rituximab-MicAbody, and median fluorescence intensity was correlated with Quantum™ MESF 647 beads (Bangs Laboratories #647).

Cell lines and *in vitro* assays. Ramos human B cell lymphoma cells (ATCC #CRL-1596) were cultured in RPMI supplemented with 20 mM HEPES and 10% FBS and regularly passaged to not exceed $1.5x10^6$ cells/mL. The mouse colon carcinoma line CT26 transfected to express human Her2 were a kind gift from Professor Sherie Morrison (UCLA).

To quantify target cell lysis, a calcein-release assay was employed. Tumor cells were centrifuged and resuspend in 4 mM probenecid (MP Biomedicals #156370) + 25 µM calcein-AM (Thermo Fisher #C1430) in T cell medium at $1\text{-}2x10^6$ cells/ml for one hour at 37°C, washed once, and adjusted to $8x10^5$ cells/ml. $CD8^+$ CAR-T cells were pelleted and resuspended in 4 mM probenecid with 60 IUe/ml IL-2 in T cell medium at $4x10^6$ cells/mL then adjusted according to the desired effector:target ratio. 25 µL target cells were plated followed by 25 µL medium or diluted MicAbody. Then 100 uL medium (minimum lysis), medium + 3% Triton-X 100 (maximum lysis), or CAR-T cells were added and plates incubated at 37°C for two hours. Experimental E:T ratios ranged from 1:1 to 20:1 and were based on absolute number of T cells, unadjusted for $\%GFP^+$ transduction efficiency. Cells were pelleted and 75 uL supernatant transferred to black clear-bottom plates and fluorescence (excitation 485 nm, emission cutoff 495 nm, emission 530 nm, 6 flashes per read) acquired on a Spectramax M2 plate reader. For experiments with armed *convertible*CAR-$CD8^+$s, T cells were pre-incubated at 37°C with either saturating

(5 nM) or a titration of MicAbody for 30 minutes before washing to remove unbound MicAbody and co-culturing with calcein-loaded target cells.

In order to quantify the target-dependent activation of T-cells, experiments were set up as described above except that calcein-preloading was omitted and assays set up in T cell medium without IL-2 supplementation. After 24 hours co-culture, supernatants were harvested and stored at -80°C until the amount of liberated cytokine could be quantified by ELISA MAX™ Human IL-2 or Human IFN-g detection kits (BioLegend #431801 and #430101).

To generate a MicAbody binding curve to iNKG2D.YA-CAR expressing T-cells, Rituximab.LC-U2S3 was labeled with Alexa Fluor 647. $3x10^5$ *convertible*CAR-CD8$^+$ cells were plated in 96-wells V-bottom plates and incubated with labeled MicAbody for 30 minutes at room temperature in a final volume of 100 uL RPMI + 1% FBS with a titration curve starting at 200 nM. Cells were then rinsed and median fluorescence intensity determined for each titration point by flow cytometry.

Animal studies. All animal studies were conducted with ProMab Biotechnologies, Inc. (Richmond, CA) with the exception of the U2S3-hFc-mutIL2 pharmacokinetic (PK) sampling which was conducted by Murigenics (Vallejo, CA). For PK analysis of serum levels of MicAbodies, six-week old female NSG mice (The Jackson Laboratory) were injected intravenously (IV) with 100 ug of either parent rituximab antibody (ADCC-), a heavy-chain U2S3 fusion of rituximab (Rituximab.HC-U2S3) or a light-chain fusion (Rituximab.LC-U2S3). Collected serum was subjected to ELISA by capturing with human anti-rituximab idiotype antibody (HCA186, Bio-Rad Laboratories), detected with rat-anti-rituximab-HRP antibody (MCA2260P, Bio-Rad), and serum levels interpolated using either a rituximab or Ritxumab-U2S3 standard curve. PK analysis of U2S3-hFc-mutIL2 was performed in NSG mice by IP injection of 60 ug followed by regular serum collection. Samples were examined by ELISA capturing with Fc-iNKG2D and detecting with biotinylated rabbit-anti-human IL-2 polyclonal antibody (Peprotech #500-P22BT) followed by incubation with streptavidin-HRP. Half-lives were calculated in GraphPad Prism based upon the beta-phase of the curve using a nonlinear regression analysis, exponential, one-phase decay analysis with the plateau constrained to zero.

For disseminated Raji B cell lymphoma studies, six-week old female NSG mice were implanted IV with Raji cells stably transfected to constitutively express luciferase from *Luciola italica* (generated and maintained by ProMab). Initiation of treatment administration is detailed in each *in vivo* study figure. For all experiments, CD4 and CD8 primary human T cells were independently transduced, combined post-expansion at a 1:1 mixture of CD4:CD8 cells without normalizing for transfection efficiency between cell types or CAR constructs, and the mixture validated by flow cytometry prior to IV injection. Administration of MicAbody or control antibody was by the intraperitoneal (IP) route unless otherwise specified, and *in vivo* imaging for bioluminescence was performed with a Xenogen IVIS system (Perkin Elmer). Animals were bled regularly to monitor human T cell dynamics by flow cytometry, staining with APC Anti-Human CD3 (clone OKT3, 20-0037-T100, Tonbo Biosciences), monitoring GFP, and examining cell-associated MicAbody levels with biotinylated Anti-Human F(ab')2 (109-066-097, Jackson ImmunoResearch Laboratories Inc.). Serum ELISAs to monitor MicAbody levels was performed as described above.

Subcutaneous Raji B cell tumor studies were performed in NSG mice implanted with $1x10^6$ Raji cells in matrigel on the right flank and tumors allowed to establish until 70-100 mm^3, at which point therapy was initiated. For the cohort that received armed *convertible*CAR-T cells, the cells were incubated with 5 nM Rituximab.LC-U2S3 MicAbody *ex vivo* for 30 minutes at room temperature before washing and final mixing to achieve the desired 1:1 CD4:CD8 ratio and cell concentration. Arming was confirmed by flow cytometry with the biotinylated Anti-Human F(ab')2 antibody and revealed a strong correlation between GFP and F(ab')2 MFIs. These mice did not receive a separate MicAbody

administration. Caliper measurements were regularly taken to estimate tumor volume, and terminal tumor masses were weighed.

Targeted delivery of complement C1q to cells expressing iNKG2D.AF-CAR. To generate Fc reagents with enhanced complement binding and targeted delivery to the T cells expressing NKG2D.AF variant receptor, the orthogonal ligand was cloned as a fusion to either the N- (U2R-Fc) or C-terminus (Fc-U2R) of human IgG1 Fc via a GGGS linker with the Fc including the hinge, CH2, and CH3 domains. In addition to the wild-type Fc, the K326A/E333A[51] (Kabat numbering, "AA") and S267E/H268F/S324T/G236A/I332E[52] ("EFTAE") C1q-enhanced binding mutation sets were explored. All were expressed in Expi293T cells, purified, and fractionated as described above. Confirmatory ELISAs were performed by capturing with Fc-NKG2D.AF followed by binding U2R/Fc-variant fusions at 1 ug/mL concentration, titrating in human-C1q protein (Abcam #ab96363), then detecting with polyclonal sheep-anti-C1q-HRP antibody (Abcam #ab46191). Complement-dependent cytotoxicity (CDC) assays were performed by iQ Biosciences (Berkeley, CA). Briefly, $5x10^4$ CD8+ cells from an NKG2D.AF-CAR transduction were plated in 96-well plates and incubated for three hours with a serial dilution of each U2R/Fc-variant fusion, in triplicate, in the presence of normal human serum complement (Quidel Corporation) at a final concentration of 10% (v/v). Cells were then harvested and resuspended with SYTOX™ Red dead cell stain (Thermo Fisher) at a final concentration of 5 ug/mL and analyzed by flow cytometry. EC_{50} values for cytotoxicity were calculated in GraphPad prism fitted to a non-linear regression curve.

Targeted delivery of mutant-IL2 to T cells expressing iNKG2D-CAR. To generate a reagent that was monomeric for the U2S3 ligand, monomeric for a mutant IL-2 with significantly reduced IL-2Rα binding (mutIL2, R38A/F42K)[53 54], yet retained serum stability, a heterodimeric Fc strategy was employed[55]. U2S3 was fused to the N-terminus of the Fc-hinge of one chain with K392D/K409D (Kabat numbering) mutations while the mutIL2 was fused to the C-terminus of the second Fc-chain which harbored E356K/D399K mutations. Additionally, D265A/N297A mutations were introduced in both Fc chains to render the Fc ADCC-deficient. Expression in Expi293T cells and purification was as described above. Appropriately assembled U2S3-hFc-mutIL2 material was fractionated by SEC and the presence of individual size-appropriate polypeptides was confirmed by denaturing SDS-PAGE. A direct fusion between orthogonal ligand and mutIL2 expressed as a single polypeptide with a linker comprising glycine-serine linkages, a FLAG tag, and a 6xHis tag was also generated and purified by Ni-NTA exchange chromatography[56]. Determination of IUe activity equivalents was based on the calculation that a 4.4 uM

---

[51] E. E. Idusogie et al., "Engineered Antibodies with Increased Activity to Recruit Complement," *Journal of Immunology (Baltimore, Md.: 1950)* 166, no. 4 (February 15, 2001): 2571–75.
[52] Gregory L. Moore et al., "Engineered Fc Variant Antibodies with Enhanced Ability to Recruit Complement and Mediate Effector Functions," *MAbs* 2, no. 2 (April 2010): 181–89.
[53] K. M. Heaton, G. Ju, and E. A. Grimm, "Human Interleukin 2 Analogues That Preferentially Bind the Intermediate-Affinity Interleukin 2 Receptor Lead to Reduced Secondary Cytokine Secretion: Implications for the Use of These Interleukin 2 Analogues in Cancer Immunotherapy," *Cancer Research* 53, no. 11 (June 1, 1993): 2597–2602.
[54] K. Sauvé et al., "Localization in Human Interleukin 2 of the Binding Site to the Alpha Chain (P55) of the Interleukin 2 Receptor," *Proceedings of the National Academy of Sciences of the United States of America* 88, no. 11 (June 1, 1991): 4636–40.
[55] Kannan Gunasekaran et al., "Enhancing Antibody Fc Heterodimer Formation through Electrostatic Steering Effects: Applications to Bispecific Molecules and Monovalent IgG," *The Journal of Biological Chemistry* 285, no. 25 (June 18, 2010): 19637–46, https://doi.org/10.1074/jbc.M110.117382.
[56] Reza Ghasemi et al., "Selective Targeting of IL-2 to NKG2D Bearing Cells for Improved Immunotherapy," *Nature Communications* 7 (21 2016): 12878, https://doi.org/10.1038/ncomms12878.

solution of wild-type IL-2 has the equivalent of 1000 IU/uL. IL-15 with a V49D mutation, which reduced binding to IL15R-alpha but retained bioactivity[57], was similarly formatted with U2S3.

CAR-T cell proliferation in response to various cytokines or U2S3-cytokine fusions was quantified with the WST-1 Cell Proliferation Reagent (Millipore Sigma #5015944001). Briefly, CAR-T cells were pelleted and resuspended in T cell media without IL-2, dispensed into 96-well plates at $4x10^4$ cells/well, and the appropriate amount of diluted U2S3-cytokine fusions was added to achieve 30 IUe/mL or higher concentration as needed in a final assay volume of 100 uL per well. Recombinant-human IL2 and IL15 (Peprotech #200-02 and #200-15) were included as controls. After incubation for three days at 37°C, 10 uL of WST-1 was added to each well and allowed to incubate for 30-60 minutes before quantifying intensity of color development on a plate reader. Changes in the proportion of GFP+ CAR-expressing cells in response to U2S3-cytokine fusion were monitored by flow cytometry.

Human PBMC stimulation and immune-phenotyping studies were performed by iQ Biosciences. Briefly normal PBMCs from three donors were seeded in 96-well plates at $1x10^5$ cells/well and exposed to a 10-fold dilution series of either U2S3-hFc-mutIL2 or U2S3-hFc-wtIL2 (wild-type IL2) for four days at 37°C with 5% CO_2. Positive controls included wells coated with anti-human CD3 (OKT2) at 2 ug/mL and rhIL-2 at 300 IUe/mL. After incubation, cells were treated with TruStain FcX block (BioLegend #422301) followed by staining with BioLegend antibody panels for proliferating T cells (CD8 clone RPA-T8 #301050, CD4 clone OKT4 #317410, CD3 clone OKT3 #300430, KI-67 #350514), regulatory T cells (Fox3 clone 206D #320106, CD4 clone OKT4, CD3 clone OKT3, KI-67), and NK cells (CD56 clone HCD56 #362546, CD3 clone OKT2, KI-67).

Immunogenicity profiling. Potential immunogenicity of NKG2D and ULBP2 mutations was analyzed with the NetMHC 4.0 Server (http://www.cbs.dtu.dk/services/NetMHC/) which uses artificial neural networks to calculate the likelihood of peptide-MHC class I binding[58]. Sequences including the 10 residues on either side of the mutation(s) of both the wild-type and mutant candidate peptides were submitted and a 9-mer moving window analyses were performed against an *in silico* peptide-MHC library using the supertype representative of each HLA haplotype. The data were compiled and simplified to show only the predicted nM affinity and % rank; strong binders are defined as having a % rank < 0.5 and weak binders a % rank < 2. For analysis of peptide binding to MHCII, the NetMHCII 2.3 Server was used (http://www.cbs.dtu.dk/services/NetMHCII/) which also uses artificial neural networks to predict peptide binding to nine HLA-DP, 20 HLA-DQ, and 25 HLA-DR alleles[59]. Sequences including the 15 residues flanking the mutation(s) of wild-type, and mutant candidates were submitted. The 15-mer moving window analyses were performed using default parameters. The prediction values for peptide binding to any given haplotype are reported as nM IC50 values and strong and weak binding peptides are specified in the program output. See Supplementary Tables for compiled prediction outputs.

---

[57] Jérôme Bernard et al., "Identification of an Interleukin-15alpha Receptor-Binding Site on Human Interleukin-15," *The Journal of Biological Chemistry* 279, no. 23 (June 4, 2004): 24313–22, https://doi.org/10.1074/jbc.M312458200.

[58] Massimo Andreatta and Morten Nielsen, "Gapped Sequence Alignment Using Artificial Neural Networks: Application to the MHC Class I System," *Bioinformatics (Oxford, England)* 32, no. 4 (February 15, 2016): 511–17, https://doi.org/10.1093/bioinformatics/btv639.

[59] Kamilla Kjaergaard Jensen et al., "Improved Methods for Predicting Peptide Binding Affinity to MHC Class II Molecules," *Immunology* 154, no. 3 (July 2018): 394–406, https://doi.org/10.1111/imm.12889.

RESULTS

Engineering a privileged binding interaction between an inert NKG2D receptor and orthogonal ULBP2 variant

Two central tyrosine residues in each NKG2D monomer have critical roles in driving receptor engagement with the eight8 diverse natural ligands of NKG2D [60] [FIGURE 1A]. Systematic mutagenesis of NKG2D has revealed that while residues comparable in size could be substituted without significant compromise in affinity for ligands, smaller residues were less tolerated. A number of non-conservative substitutions at each tyrosine residue were made and examined for loss of binding to natural ligands and ease of expression as recombinant Fc-fused reagents. These parameters were used as metrics for prioritization; those mutants that resulted in poor expression yields or the generation of highly aggregated material were discarded as candidate receptor variants. Of the priority NKG2D mutants, the Y152A mutant ("iNKG2D.YA") and the Y152A/Y199F double mutant ("iNKG2D.AF") were selected for further characterization. Both were readily expressed and purified as recombinant proteins (data not shown) and both exhibited loss of binding to all naturally occurring human ligands as assessed by both BLI [FIGURES 2A and 5A] and ELISA [FIGURES 2B and 5B].

A phage display strategy was implemented to rapidly interrogate ligand mutants and select for those with high affinity binding to the inert NKG2D variants but not to the wild-type receptor. Orthogonal variants were identified for MICA and ULBP3 (data not shown), but ULBP2 was selected as the focus of engineering efforts since no human polymorphisms have been described[61]. The strong tertiary similarity shared by the ligands, particularly in the two alpha-helices at the interface of NKG2D interaction [FIGURE 1B], facilitated the development of a targeted mutagenesis strategy wherein libraries were generated for ULBP2 examining each alpha-helix independently or in combination. The strategy was additionally informed by the high sequence identity shared with ULBP6 [FIGURE 1C] for which structure-function information was available[62]. In initial attempts to evolve variants against iNKG2D.YA only helix 4 libraries (NNK at residues 156-160) yielded orthogonal variants as helix 2 libraries (NNK at residues 74-78) did not return any selective variants. The combination helix 2/helix 4 library only returned mutations in helix 4. Additionally, initial attempts at probing helix 4 yielded marginal iNKG2D.YA selectivity, and sequencing of candidates revealed deletions and frameshifts in the mutated region except when R81W was spontaneously present (data not shown). This suggested a stabilizing role for the R81W mutation, supported by its location at the C-terminus of helix 2. As a consequence, all ULBP2 libraries were generated with the R81W mutation incorporated. Competitive selection with rounds of increasing concentration of wild-type NKG2D resulted in several phage candidates that selectively engaged iNKG2D.YA [FIGURE 3A]. Sequencing of isolates revealed three independent sequence variants – U2S1, U2S2, and U2S3 – that reproducibly bound iNKG2D.YA [FIGURE 3B]. All three were cloned as fusions to the C-terminus of the IgG1 heavy chain of the anti-FGFR3 antibody clone R3Mab to generate a bispecific reagent and were demonstrated by ELISA to retain NKG2D.YA selectivity orthogonal to wild-type ULBP2 [FIGURE 3C]. Interestingly, the R81W mutation alone recovered affinity towards wtNKG2D and yet retained binding to iNKG2D.YA [FIGURES 3C and 4A]. However, the presence of the R81W mutation in the iNKG2D-selective variants was essential since its reversion to the wild-type

---

[60] Culpepper et al., "Systematic Mutation and Thermodynamic Analysis of Central Tyrosine Pairs in Polyspecific NKG2D Receptor Interactions."

[61] Lola Fernández-Messina, Hugh T. Reyburn, and Mar Valés-Gómez, "Human NKG2D-Ligands: Cell Biology Strategies to Ensure Immune Recognition," *Frontiers in Immunology* 3 (2012): 299, https://doi.org/10.3389/fimmu.2012.00299.

[62] Zuo et al., "A Disease-Linked ULBP6 Polymorphism Inhibits NKG2D-Mediated Target Cell Killing by Enhancing the Stability of NKG2D Ligand Binding."

residue resulted in loss of binding to iNKG2D.YA (data not shown). Variant U2S3 consistently showed a greater binding differential so was more thoroughly examined kinetically. As a monomer, U2S3 had a 10-fold higher affinity towards iNKG2D.YA than wild-type ULBP2 had to wtNKG2D [FIGURE 4A]. In the context of a rituximab antibody fusion bivalent for the U2S3 ligand, picomolar affinity towards iNKG2D.YA was measured with complete retention of orthogonality in both the light-chain (LC) and heavy-chain (HC) fusion configurations [FIGURE 4B]. Size-exclusion chromatography of both the HC and LC Rituximab-MicAbody fusions revealed a predominant species with a small amount of higher molecular weight material. After fractionation the predominant material migrated at a slightly shifted peak relative to the parental rituximab (ADCC-) antibody, consistent with the expected higher molecular weight of the fusion protein [FIGURE 4C]. Thermal stability characterization revealed that inclusion of U2S3 as either a HC or LC fusion did not alter the stability of either MicAbody relative to the parent antibody [FIGURE 4D].

BLI characterization of iNKG2D.AF binding to wild-type monomeric ligands revealed a reduction in binding and affinity of all ligands relative to wtNKG2D [FIGURE 5A]. The same helix 2, helix 4, and combination helix 2/helix 4 libraries (with R81W already incorporated) were generated and panned against Fc-iNKG2D.AF with Fc-wtNKG2D competition. Similar to Fc-iNKG2D.YA panning, only the helix 4 library yielded significant enrichment with the combination library returning only helix 4 mutants. Candidate mutants were expressed as LC fusions to rituximab, and ELISA assays were performed comparing binding to Fc-wtNKG2D, Fc-iNKG2D.YA, and Fc-iNKG2D.AF in order to identify those that could discriminate between iNKG2D.AF and both wtNKG2D and iNKG2D.YA. Four candidates were identified that retained high affinity engagement of iNKG2D.AF but did not engage either of the other two receptors [FIGURE 5B]. Of these four, U2R [FIGURE 1C] was selected as the primary iNKG2D.AF orthogonal U2 variant since it had virtually undetectable levels of binding to wtNKG2D and iNKG2D.YA. ELISAs were performed to directly compare binding of Rituximab.LC-U2S3 and Rituximab.LC-U2R to both iNKG2D.YA and iNKG2D.AF. The results confirmed that two independent orthogonal ligands were identified, each of which exclusively engaged the inert NKG2D variant for which it was evolved [FIGURE 5C].

The potential immunogenicities of the iNKG2D variants and ULBP2 variants were determined using *in silico* prediction analysis tools that scored the binding affinities of peptides to MHC since this correlates with peptide immunogenicity[63]. Both the iNKG2D.YA and iNKG2D.AF mutations were predicted to be no more immunogenic than the corresponding wild-type peptide across all of the human haplotypes available for analysis [SUPPLEMENTARY TABLES]. Additionally, all mutations incorporated into the U2S3 orthogonal ligand and the U2R orthogonal ligand were also predicted to be no more immunogenic than the natural peptides.

Expression of iNKG2D.YA as a chimeric antigen receptor on T cells

FIGURE 6A summarizes the engineering steps and CAR components involved in generating the exclusive receptor-ligand interaction and the mechanism behind flexible antigen targeting. The iNKG2D.YA was expressed as a second generation CAR receptor tethered to the CD8-alpha hinge and transmembrane domain, 4-1BB, and CD3zeta. Additionally, a C-terminal eGFP fusion was included for monitoring expression efficiency and to facilitate *in vivo* tracking of CAR cells [FIGURE 6B]. The construct was transduced into primary human CD4 and CD8 T cells using a second generation lentivirus-based vector system to generate iNKG2D.YA-CAR-T cells, termed *convertible*CAR-T cells. The expression levels of the iNKG2D CARs were comparable to a rituximab scFv-based CAR construct (RITscFv-CAR) which other than the scFv was identical in architecture to the iNKG2D.YA-CAR [FIGURE 6C]. Transduction efficiency varied between donors and lentiviral preps, but >70% GFP+ yields were consistently achieved

[63] Jensen et al., "Improved Methods for Predicting Peptide Binding Affinity to MHC Class II Molecules."

(data not shown). In addition, staining of surface iNKG2D.YA with the Rituximab.LC-U2S3 MicAbody correlated strongly with GFP expression, suggesting a direct relationship between efficiency of expression and presentation on the surface [FIGURE 6D]. A median of 21,000 molecules of iNKG2D.YA-receptors was estimated using fluorescent calibration beads to be on surface of the transduced T cells. The *convertible*CAR-T cells are incapable of engaging target cells on their own but instead can be directed towards an antigen-expressing target only when armed with the appropriate MicAbody [FIGURE 6A].

To demonstrate that iNKG2D.YA specificity of the orthogonal U2S3 ligand was retained even in the context of a CAR-T cell, CD8 T cells expressing either a iNKG2D.YA-CAR or a wild-type NKG2D CAR (wtNKG2D-CAR) were exposed to wells of a microtiter plate coated with different concentrations of the monomeric wild-type MIC or U2S3 ligands. After 24 hours, the supernatants were harvested and the amount of IL-2 and IFNγ cytokine released was quantified by ELISA. Although cells expressing wtNKG2D-CAR were activated and produced cytokines in response to wild-type MIC ligands, they did not respond to U2S3, even at the highest orthogonal ligand densities [FIGURE 7A]. INKG2D.YA-CAR expressing cells, on the other hand, liberated cytokines only when presented to U2S3 and did so in a concentration-dependent manner. Introduction of a target cell, on its own, was insufficient to drive activation of iNKG2D.YA-CAR cells when in the presence of Ramos (CD20+) target cells [FIGURE 7B]. Instead the appropriate antigen-targeting MicAbody is absolutely required as neither rituximab antibody nor Trastuzumab.LC-MicAbody was able to activate CAR cells even at very high concentrations. These data demonstrated that the formation of an immunological synapse with CAR receptor clustering was required for activation of *convertible*CAR-bearing cells either in the context of U2S3 being directly presented as a two-dimensional array on a solid surface or bound to the surface of an antigen-bearing target cell. Maximum cytokine release was achieved when the concentration of the MicAbody was in the 32-160 pM range. Furthermore, activation of CAR-T cell function was dependent upon the presence of the appropriate cognate ULBP2 variant. Specifically, Rituximab.LC-U2R MicAbody did not promote lysis of Ramos cells by iNKG2D.YA CAR-T cells although Rituximab.LC-U2R MicAbody did enable iNKG2D.AF-CAR cells to eliminate targeted cells [FIGURE 5D].

The pM levels of MicAbody needed to stimulate maximal cytokine production prompted additional characterization regarding occupancy of iNKG2D-CAR receptors on the surface of the cell by MicAbodies and relating the occupancy to T cell function. Staining of *convertible*CAR CD8+ cells with a fluorescently labeled Rituximab.LC-U2S3 MicAbody revealed saturation of iNKG2D.YA-CAR receptors at 5 nM [FIGURE 8A]. Using this as a starting point, *convertible*CAR CD8+ cells were incubated with decreasing amounts of Rituximab.LC-U2S3, excess MicAbody was removed, and the extent of lysis of Ramos target cells determined by calcein release. Cell lysis remained close to maximum for the assay until the concentration used in arming was below 30 pM [FIGURE 8B]. Saturation of surface-expressed iNKG2D.YA was achieved at 5nM, 30 pM was the inflection point for maximal cytolysis, and maximal activation occurred in the low pM range. There is therefore a two-order of magnitude difference between the concentration of cognate MicAbody required for full activation of cellular function and complete occupancy of the receptors. This suggested that there was potential for arming the *convertible*CAR-cell with more than one MicAbody, thereby directing its activity to multiple targets simultaneously. To directly test this, *convertible*CAR CD8+ cells were armed with Rituximab.LC-U2S3, Trastuzumb.LC-U2S3 (targeting Her2), or an equimolar mixture of the two MicAbodies and exposed to either Ramos cells or CT26 cells that had been transfected to express human Her2. Although CAR cells armed with a single MicAbody directed lysis to only tumor cells expressing the cognate antigen, dual-armed CARs targeted both tumor cell lines without compromising lytic potency against either target-expressing cell, thereby demonstrating multiplex capabilities of *convertible*CAR-T cells [FIGURE 8C].

***convertible*CAR-T cells inhibit expansion of a disseminated B-cell lymphoma.**

The pharmacokinetics of both the HC and LC Rituximab-U2S3 MicAbodies [FIGURE 9A] revealed a steeper alpha-phase than the parental ADCC- antibody due to the fact that U2S3 can still bind wild-type mouse NKG2D (data not shown). However, once the mouse NKG2D sink was occupied, the beta-phase of both MicAbody formats resembled the parent with the LC-U2S3 fusion perhaps having a slightly longer half-life than the HC-fused MicAbody. The LC fusion also out-performed the HC fusion in an *in vitro* killing assay with Ramos target cells [FIGURE 9B]. In an *in vivo* comparison of the two MicAbody formats in NSG mice [FIGURE 9C], Rituximab.LC-U2S3 was perhaps more efficacious at early time points than Rituximab.HC-U2S3 in controlling the expansion of disseminated Raji B cell lymphoma [FIGURE 9D]. Both MicAbody formats were much more efficient at controlling the tumor than *convertible*CAR cells alone or in combination with rituximab antibody. As a consequence of the preferred PK property, improved *in vitro* killing, and greater *in vivo* tumor control, the LC fusion format of Rituximab-MicAbody was selected for all subsequent *in vivo* experiments.

A series of *in vivo* experiments were performed to investigate how *convertible*CAR-T cell dose, MicAbody dose, and frequency of dosing might impact the growth of a disseminated Raji lymphoma [FIGURE 10]. Rituximab-MicAbody alone was ineffective at suppressing tumor expansion - mice succumbed to disease at the same time as mice in the untreated cohort. Although 4 ug MicAbody in combination with *convertible*CAR-T cells showed early evidence of controlling the tumor, the effect was not as durable as a 20 ug dose. The 100 ug dose showed the least efficacy of the three [FIGURE 10A]. Because T cells expand after implantation and upon encountering tumor, 4 ug dose may be insufficient for maintaining the arming of *convertible*CAR-T cell productively engaging with tumor cells. The 100 ug dose may actually lead to saturation of both iNKG2D-CARs on the T cells and CD20 targets on the tumor cells, precluding sufficient receptor clustering necessary for activation. *In vitro* assays where tumor and iNKG2D-CARs were each saturated prior to co-incubation have demonstrated that tumor cell cytolysis is severely compromised (data not shown). Untransduced T cells and *convertible*CAR-T cells without MicAbody both delayed the rate at which mice succumb to tumor to the same degree and likely suppressed tumor expansion due to a combination of human donor/human tumor MHC-mismatch and the Ebstein-barr virus positive status of Raji cells. This graft-versus-tumor effect was consistently observed in our *in vivo* Raji studies, became more pronounced with greater numbers of administered untransduced cells, and likely accounted for the delay in tumor growth kinetics in control *convertible*CAR cohorts [FIGURES 10A, 10B, and 11B]. Keeping a consistent 20 ug MicAbody dose, more frequent administration at once every two days verses every four days more effectively controlled tumor growth, particularly when paired with a higher dose of ($10x10^6$) infused *convertible*CAR-T cells. Rituximab-MicAbody was detectable in the serum of mice throughout the course of the study with peak levels appearing earlier with higher frequency dosing [FIGURE 10B].

A Raji disseminated lymphoma study to optimize *convertible*CAR-T cells dosing was performed with animals dosed with Rituximab-MicAbody every two days at 20 ug and at doses of $5x10^6$ (5M) or $15x10^6$ (15M) *convertible*CAR-T cells [FIGURE 11A]. As a control, a rituximab-scFv based CAR construct (RITscFv-CAR) with the same architecture as the iNKG2D-CAR [FIGURE 6C] was also included and had been shown to have comparable *in vitro* Ramos killing activity as *convertible*CAR-T cells across all examined effector:target ratios [FIGURE 8D]. At 5M total T cells, both RITscFv-CAR and *convertible*CAR-T plus MicAbody were effective at controlling tumor expansion relative to untreated, untransduced, and *convertible*CAR-T only cohorts [FIGURE 11B]. While the average bioluminescence signal was lower for the RITscFv-CAR cohort [FIGURE 11C] than for the *convertible*CAR-T plus MicAbody group, there were clearly mice in the latter cohort that responded just as well [FIGURE 11B]. When total infused CAR-T cells was increased to 15M cells, the initial impact on tumor growth was slightly more pronounced for the RITscFv-CAR cohort while the *convertible*CAR plus MicAbody-treated mice were able to completely block tumor expansion [FIGURE 11B, 11C, and 11D]. In the disseminated model, peak levels of human CD3+ T cells consistently appeared around seven days post-infusion with the both scFv-CAR and

*convertible*CAR cells having contracted in the majority of mice by 14 days [FIGURE 11F]. There was a delayed expansion of CD3+ cells in the untransduced and *convertible*CAR-only cohorts that was contemporary with the onset of the graft-versus-tumor response and likely the consequence of select expansion of reactive clones. MicAbody associated T cells can be observed in the blood of mice in *convertible*CAR plus MicAbody cohorts [FIGURE 11G] and these cells continue to be armed as long as sufficient serum MicAbody is present (data not shown).

_convertible_CAR-T cells inhibit growth of subcutaneously implanted Raji B-cells.

Raji B-cells were implanted subcutaneously to explore the ability of the *convertible*CAR system to suppress growth of a solid tumor mass. Once tumors were established, either $7x10^6$ (7M) or $35x10^6$ (35M) *convertible*CAR-T cells were administered after a single dose of Rituximab-MicAbody [FIGURE 12A]. Additionally, one cohort received 35M cells that were armed with a saturating concentration of Rituximab-MicAbody prior to administration. The high affinity engagement between the U2S3 domain and iNKG2D.YA effectively enabled *in vitro* arming of *convertible*CAR cells that *in vivo* then became increasingly disarmed upon T cell expansion in the absence of additional MicAbody administration. Administration of MicAbody with 7M *convertible*CAR-T cells resulted in reduced tumor size relative to *convertible*CAR-T cells alone [FIGURES 12B, 12C]. Furthermore, when 35M cells were administered along with MicAbody, tumor growth was completely suppressed.

Serum levels of Rituximab-MicAbody were comparable at both CAR dose levels across the study and persisted through day 21 (11 days post-MicAbody infusion) when it was detected at approximately 600 ng/mL (3.2 nM) [FIGURE 12D]. By two days post-infusion, *convertible*CAR-T cells armed *in vitro* did not have detectable surface associated MicAbody [FIGURE 12E], a result of rapid disarming as a consequence of activation-induced cell proliferation and receptor turnover. In cohorts that received an independent systemic boost of MicAbody, its presence in serum at day 21 led to a high level of arming of peripheral T cells. By day 45 of the study (35 days post-MicAbody infusion), the cohort receiving 35M CAR-T cells plus MicAbody maintained relatively high CD3+ T cell numbers but were not well-armed with MicAbody while the 7M+MicAbody cohort did have few cells that maintained high levels of surface-associated MicAbody. This suggested that as MicAbody levels fell below detectable limits in the serum, the levels were insufficient to effectively maintain arming when cell levels are high. An alternative possibility is that the higher CD3+ cell numbers in the 35M+MicAbody cohort reflect expansion of a graft-vs-host subset of cells that do not express the CAR construct. However, the elevated CD3+ numbers were not seen in the 35M armed cohort suggesting that this is not the case. In summary, pre-armed *convertible*CAR-T cells armed *in vitro* before administration were able prior to disarming to exert a robust initial anti-tumor response that arrested tumor expansion. Furthermore, *convertible*CAR-T cells were able to effectively control a solid lymphoma in a CAR-cell dose-dependent manner when high serum level of Rituximab-MicAbody was maintained to re-arm *convertible*CAR-T cells *in vivo*.

Targeted delivery of CDC-enhanced Fc domains effectively reduces *convertible*CAR-T cell levels

The highly selective interaction engineered between the iNKG2D variants and their orthogonal ligands enables the selective delivery of agents to *convertible*CAR-T cells simply by fusing agents as payloads to the ligands themselves. We wanted to use this feature to develop a means of selectively reducing numbers of *convertible*CAR-T cells utilizing the human complement system since this is likely to remain intact in treated patient populations and effects cytolysis extrinsically. To do so, the ULBP2.R (U2R) variant selective for the iNKG2D.AF variant was fused to either the N-terminus or C-terminus of the Fc-domain of human IgG1 [FIGURE 13A]. Two sets of mutations in the CH2 domain of the Fc previously identified to enhance binding of C1q (the first component of the classical pathway for complement activation) were also introduced - S267E/H268F/S324T/G236A/I332E ("EFTAE") and K326A/E333A ("AA"). Regardless of orientation of the U2R ligand, the two molecules with wild-type Fc

bound C1q similarly with an average Kd of 0.67 nM [FIGURE 13B]. Incorporation of the AA mutations shifted C1q binding for both orientations to a slightly higher affinity (Kd of 0.35 nM) while the EFTAE set of mutations shifted binding to an even higher affinity (Kd of 0.12 nM). When untransduced $CD8^+$ T cells were incubated in a complement-dependent cytotoxicity assay with increasing combinations of U2R/Fc fusions in the presence of normal human serum, there was very little cytotoxicity detected. However, in cells transduced to express the iNKG2D.AF-CAR, cytotoxicity of the CAR-cell was observed in a concentration-dependent manner with the EFTAE variant leading to the greatest extent of killing followed by the AA variant and no detectable killing by the wild-type Fc. Interestingly, orientation of the U2R fusion was critical; C-terminal fusions did not appreciably direct killing, whereas N-terminal fusions - which orient the Fc in a manner more similar to an antibody binding a target - did direct CDC activity. Similar results with the EFTAE variant out-performing wild-type Fc was also observed with the U2S3 and iNKG2D.YA pairing (data not shown).

Selective delivery of cytokine fusions promote *convertible*CAR-T cell expansion

The potential ability of orthogonal ligands to deliver cytokines selectively to *convertible*CAR-T cells has significant advantages to not only promote their expansion but also potentially leverage differential cytokine signaling to control T cell phenotype and function. As a general design principal for this strategy, mutant cytokines with reduced binding to their receptor complexes were employed to reduce their non-selective engagement with immune cells not expressing the CAR, minimize potential immunosuppressive effects, and to also alleviate potential toxicity associated with systemic delivery of therapeutic wild-type cytokines. To this end the R38A/F42K mutations in IL-2 (mutIL2) and the V49D mutation in IL-15 (mutIL15) dramatically reduce binding to each cytokine's respective Rα subunit while maintaining IL-2Rβ/γ complex engagement. Additionally, the mutant cytokines were kept monovalent to eliminate avidity as a driving influence in IL-2Rβ/γc binding. Initial experiments using the iNKG2D.YA cognate orthogonal variant U2S2 fused to either mutIL2 or mutIL15 promoted proliferation of *convertible*CAR-expressing cells but not T cells engineered to express a CAR construct in which the NKG2D domain was wild-type [FIGURE 14A]. Furthermore, if the ULBP2.R81W mutation was employed – which does not discriminate between wild-type NKG2D and iNKG2D – both T cell populations expanded. The ability of the CAR cells to expand in response to the ligand-cytokine fusions occurred whether the molecules were directly fused to one another (e.g. U2S2-mutIL2) or if they were attached via a heterodimeric Fc linkage (e.g. U2S2-hFc-mutIL2), since both fusion molecules were in culture able to drive expansion of GFP+ *convertible*CAR-T cells to densities above the untransduced cells present [FIGURE 14B]. Ligand engagement of iNKG2D.YA alone either in the form of a MicAbody [FIGURE 7B] or a monovalent U2S3-hFc (without a cytokine payload) was insufficient to drive proliferation of *convertible*CAR-CD8 cells (data not shown), and cells maintained in the presence of a mutIL2 fusion were shown in a MicAbody-mediated killing assay to be as cytolytic as their counterparts maintained with wild-type IL-2 (data not shown).

The nature of wild-type and ligand-cytokine fusion signaling was explored by examining the phosphorylation of STAT3 and STAT5 by flow cytometry. Addition of wild-type IL-2 or IL-15 cytokines resulted in an increase of phospho-STAT3 and phospho–STAT5 (pSTAT3 and pSTAT5, respectively) in both untransduced as well as *convertible*CAR-CD8 cells [FIGURE 14C]. Treatment of untransduced cells with U2S3-hFc-mutIL2 resulted only in a minimal shift in pSTAT5 relative to the no cytokine control, consistent with mutIL2's retention of IL-2Rβ/γc binding. The *convertible*CAR-CD8 cells responded to both U2S3-hFc-mutIL2 and –mutIL15 with an increase in pSTAT5 levels via γ-chain activation of JAK3. Unlike wild-type cytokines, no increase in pSTAT3 signal was observed, indicating a reduction in JAK1

activation through IL-2Rβ[64] in both scenarios as a consequence of disruption of Rα binding, a hypothesis supported by IL-15Rα's role in increasing the affinity of IL-15 for IL-2Rβ[65]. Since the responses to both U2S3-hFc-mutIL2 and U2S3–mutIL15 were very similar, both cytokine-fusions were examined in a time-dependent manner. In both cases, treatment with ligand-cytokine fusions led to nearly identical increases at 30 minutes and diminishing thereafter. As a consequence of the similar signaling profiles for the –mutIL2 and –mutIL15 fusion molecules, only U2S3-hFc-mutIL2 was further characterized.

The heterodimeric-Fc format, defective for FcγR binding and confirmed to retain FcRn binding, (data not shown) was used for *in vivo* experimentation to leverage the enhanced serum stability of an Fc linkage. PK analysis in NSG mice revealed a half-life of 2.6 days [Figure 15A]. *convertible*CAR-T cells injected into NSG mice in the absence of tumor underwent a homeostatic expansion, peaking at three days followed by contraction. Three injections of U2S3-hFc-mutIL2 staged one week apart resulted in a dramatic expansion of human T cells in the peripheral blood [FIGURE 15B]. After cessation of U2S3-hFc-mutIL2 support, T cells numbers contracted. While CD4+ T cells did expand somewhat (data not shown), the majority of expansion was by CD8+ T cells. Furthermore, the proportion of GFP+ CD8+ T cells increased to 100% in parallel with the T cell expansion, demonstrating selective expansion of iNKG2D-CAR expressing cells and not untransduced cells [FIGURE 16C].

The effect of U2S3-hFc-mutIL2 on normal human PBMCs from three donors was explored *in vitro* by exposure to increasing concentrations of the agent for four days followed by flow-based quantification of cells positive for the proliferative marker Ki-67. In addition to the mutIL2 fusion, a version of the molecule with a wild-type IL2 (U2S3-hFc-wtIL2), which should engage both IL-2Rα/IL-2Rβγ and IL-2Rβγ independent of the U2S3 ligand, was included as a control to directly demonstrate that the reduction in IL-2 bioactivity was a consequence of the mutations employed and not the fusion format itself. CD4+ and CD8+ T cells responded robustly to both anti-CD3 and wild-type IL-2 positive controls as well as to the lowest dose of U2S3-hFc-wtIL2. Proliferative responses to U2S3-hFc-mutIL2 occurred in a dose-dependent manner with expansion observed across donors at levels above 300 IUe/mL but not achieving levels comparable to those of the IL-2 positive control until 30,000 IUe/mL, a 100-fold higher concentration. Treg responses were comparable to that of CD4+ and CD8+ cells with the exception of cells from one donor that responded to U2S3-hFc-mutIL2 at a lower concentration than the others and also had a muted response to anti-CD3 stimulation. NK cells proliferated robustly in response to IL-2 and at diminished levels to anti-CD3 stimulation as expected. However, unlike CD4+ and CD8+ responses, NK cells seemed to be less sensitive to U2S3-hFc-wtIL2 with a dose-dependent increase in proliferation that was also paralleled by a dose-dependent U2S3-hFc-mutIL2 responsiveness. Taken together, these data support the hypothesis that normal human PBMCs do not respond to U2S3-hFc-mutIL2 except at super-physiologic/pharmacologic levels and that there is a dosing window that will permit highly selective delivery of orthogonal ligand-fused mutIL2 to iNKG2D-CAR-expressing cells and avoid toxicities and Treg cell activation associated with systemic delivery of pharmacologic doses of IL-2.

DISCUSSION

We have described the engineering of a unique, highly privileged receptor-ligand (iNKG2D.YA-U2S3) pairing for the primary purpose of generating the components for a universal CAR, the versatility of which has resulted in a modular platform that is broadly controllable from the cell exterior. The iNKG2D-CAR receptor itself is invariant on T cells, and T cell function can be readily directed to

---

[64] T. Miyazaki et al., "Functional Activation of Jak1 and Jak3 by Selective Association with IL-2 Receptor Subunits," *Science (New York, N.Y.)* 266, no. 5187 (November 11, 1994): 1045–47.

[65] Aaron M. Ring et al., "Mechanistic and Structural Insight into the Functional Dichotomy between IL-2 and IL-15," *Nature Immunology* 13, no. 12 (December 2012): 1187–95, https://doi.org/10.1038/ni.2449.

potentially any antigen of interest by virtue of attaching the orthogonal ligand to the appropriate antigen-recognizing antibody. In this manner, the same iNKG2D-CAR-expressing T cell can be retargeted as needed if, for example, the original tumor antigen becomes downregulated during the course of therapy. This targeting flexibility is not limited to sequential engagement of antigens, but can also be multiplexed to simultaneously direct T cells to more than one antigen expressed on a single cancer cell in order to greatly reduce the likelihood of tumor escape. Targeting more than one antigen simultaneously within the tumor can also address the issue of heterogeneity of tumor antigen expression. Additionally, this multiplexing approach can be used to leverage activity against different cell types within the tumor microenvironment to promote not only destruction of cancer cells, but also of additional cell types whose removal would enhance overall tumor reduction. The use of MicAbodies provides an opportunity to differentially engage and activate *convertible*CAR-T cells, distinguishing them from scFv-CARs that are generally committed to a fixed level of receptor expression and hence reduced ability to discriminate between different antigen levels present on healthy versus aberrant cells. The demonstrated dose-dependency of *convertible*CAR-T cells for both cytolysis and activation provides the prospect of administering MicAbody in a manner that would best integrate variable tumor burdens and antigen densities to achieve a therapeutic index sufficient to reduce the risk of adverse events – such as cytokine release syndrome (CRS) and neurotoxicity (NTX).

Another significant advantage of this privileged receptor-ligand interaction is that the orthogonal ligand can be fused to an innumerable variety of payloads for delivery specifically to iNKG2D-bearing cells to effect outcomes without having to engineer additional systems within the cell. The exogenous control of cell quantity and activity includes the ability to harness the breadth of interleukin functions to drive expansion and activation, prevent exhaustion, or even promote suppression in a controlled and targeted manner. By implementing the general design principle of using mutant cytokines with reduced bioactivity to minimize non-specific effects, we have demonstrated the selective activity of both mutIL2 and mutIL15 in driving *convertible*CAR-T expansion in vitro and in vivo. Introduction of cytokine-ligand fusions during the CAR manufacturing process could increase the overall yield of patient T cells and compensate for low transduction efficiencies. Once the CAR-cells have been administered to the patient, cytokine-ligand fusions could be administered early on to increase the number of CAR-T cells in the patient which, with CD19-CAR therapies, is correlated with response rates[66]. Most CAR therapies require a preconditioning lymphodepletion regimen to promote engraftment and expansion of CAR cells. One rationale for lymphodepletion is to provide a more verdant immunological setting for CARs to expand[67]. Robust and controllable *convertible*CAR expansion in patients may supplant the need for lymphodepletion, allowing for retention of endogenous immune functions that are fully competent to support the initial *convertible*CAR-mediated anti-tumor activity, especially since all the components of the *convertible*CAR system (with the exception of antibody Fv domains) are of minimally altered, human origin. Because *convertible*CAR-Ts are functionally inert without their targeting MicAbody, it should be safe to drive their expansion to a level that would maximize anti-tumor activity upon MicAbody administration. Another clinical strategy might be to deliver cytokine-ligand fusions to bolster *convertible*CAR-T function, possibly with a cycling regimen to

[66] Joseph A. Fraietta et al., "Determinants of Response and Resistance to CD19 Chimeric Antigen Receptor (CAR) T Cell Therapy of Chronic Lymphocytic Leukemia," *Nature Medicine* 24, no. 5 (2018): 563–71, https://doi.org/10.1038/s41591-018-0010-1.

[67] Kevin A Hay and Cameron J Turtle, "Chimeric Antigen Receptor (CAR) T Cells: Lessons Learned from Targeting of CD19 in B Cell Malignancies," *Drugs* 77, no. 3 (March 2017): 237–45, https://doi.org/10.1007/s40265-017-0690-8.

reduce T cell exhaustion and promote the maintenance of memory T cells[68]. And lastly, CARs have been demonstrated to persist in humans for years post-infusion[69], the ability to recall resident *convertible*CAR-Ts to attack the original tumor or even mount an attack on metastases or a second, independent tumor (either with the original targeting MicAbody or a different one) without having to re-engineer or generate a new batch of CAR cells should be highly advantageous. Unlike scenarios where CAR cells are engineered to constitutively express cytokines[70] [71], delivery of cytokines exclusively to *convertible*CAR cells can be modulated depending upon the manufacturing or clinical needs.

The functional consequence of eliminating IL-2Rα and IL-15Rα binding of IL-2 and IL-15, respectively, is that their signaling interaction is limited to the shared IL-2Rβ/γc. It is therefore not surprising that both the mutIL2- and mutIL15-ligand fusions result in the similar outcomes with regard to both levels of proliferation *in vitro* and diminution of STAT3 phosphorylation while maintaining STAT5 signaling. Indeed the overall signaling effects of both IL-2 and IL-15 in the context of their fully functional trimeric receptors are remarkably similar, with their respective alpha subunits ultimately driving cellular responsiveness that is likely both context-dependent (location of Rα expression) and kinetically driven (defined by differential affinities of each respective cytokine for its Rα)[72]. In a contrived setting where cytokines are engineered to selectively engage a CAR cell, there are additional considerations when designing a cytokine with reduced bioactivity, and simple reduction in overall receptor affinity may not be sufficient if distinct outcomes with different cytokines is desired. There is much mutational space that can be explored in the context of cytokines in order to differentially promote signaling outcomes, exemplified by IL-2 variants that have been described to differentially engage the IL-2Rβ and IL-2Rγc subunits and drive different amplitudes of agonistic and antagonistic effects[73]. Additionally, the heterodimeric-Fc chassis that we have developed is amenable to the incorporation of multiple cytokine subunits in order to deploy a strategy that combines multiple cytokines such as IL-21 and IL-15, the outcome of which would be to enhance memory and naïve CD8 subsets[74].

We have also demonstrated the feasibility of leveraging the receptor-ligand interaction to deliver Fc-domains with enhanced complement C1q binding for attrition of *convertible*CAR-T cells. The strategy of co-expressing an epitope such as a truncated EGFR (EGFRt) or CD20 on CAR cells for the purpose of harnessing antibody-mediated killing by administration of the appropriate antibody (e.g.

---

[68] Sophie Viaud et al., "Switchable Control over in Vivo CAR T Expansion, B Cell Depletion, and Induction of Memory," *Proceedings of the National Academy of Sciences of the United States of America* 115, no. 46 (13 2018): E10898–906, https://doi.org/10.1073/pnas.1810060115.

[69] David L. Porter et al., "Chimeric Antigen Receptor T Cells Persist and Induce Sustained Remissions in Relapsed Refractory Chronic Lymphocytic Leukemia," *Science Translational Medicine* 7, no. 303 (September 2, 2015): 303ra139, https://doi.org/10.1126/scitranslmed.aac5415.

[70] Hurton et al., "Tethered IL-15 Augments Antitumor Activity and Promotes a Stem-Cell Memory Subset in Tumor-Specific T Cells."

[71] Mauro P. Avanzi et al., "IL-18 Secreting CAR T Cells Enhance Cell Persistence, Induce Prolonged B Cell Aplasia and Eradicate CD19+ Tumor Cells without Need for Prior Conditioning," *Blood* 128, no. 22 (December 2, 2016): 816–816.

[72] Ring et al., "Mechanistic and Structural Insight into the Functional Dichotomy between IL-2 and IL-15."

[73] Suman Mitra et al., "Interleukin-2 Activity Can Be Fine Tuned with Engineered Receptor Signaling Clamps," *Immunity* 42, no. 5 (May 19, 2015): 826–38, https://doi.org/10.1016/j.immuni.2015.04.018.

[74] Rong Zeng et al., "Synergy of IL-21 and IL-15 in Regulating CD8+ T Cell Expansion and Function," *The Journal of Experimental Medicine* 201, no. 1 (January 3, 2005): 139–48, https://doi.org/10.1084/jem.20041057.

cetuximab or rituximab, respectively) [75] [76] [77] has led to the successful depletion of CAR cells in preclinical models but is reliant on clinically approved antibodies that will likely have collateral effects including toxicity due to cytolysis of opsonized healthy cells, in the case of rituximab, B-cell aplasia. The advantage of our strategy is that we have utilized solely the Fc-portion of IgG1 that has been mutated to enhance complement-mediated killing and will therefore have effects exclusively on cells expressing iNKG2D on their surface.

By design, each component of the *convertible*CAR system – the iNKG2D-based CAR receptor and the MicAbody – are functionally inert on their own. This has significant advantages during manufacturing, particularly in the context of indications such as T cell malignancies where traditional scFv-based CARs encounter expansion hurdles due to fratricide[78]. Additionally, it provides enhanced control of CAR function during treatment. *convertible*CAR-T cells could be armed with MicAbody prior to administration, thus providing the benefit of an initial burst of anti-tumor activity on par with traditional scFv-CARs. However, the *convertible*CAR-T cells will replicate, which reduces the amount density of surface-associated MicAbody. The 4-1BB/CD3zeta scFv-CARs have also been shown to rapidly and dramatically internalize their CARs upon antigen engagement and we would expect the same to happen with the iNKG2D-CAR receptors since they share a similar signaling architecture[79]. As a consequence of these two processes, *convertible*CAR-T cells will rapidly disarm after initial expansion and target engagement, which then provides an opportunity rearm and re-engage tumor in a manner controlled by MicAbody dosing to optimize tumor cytolysis and mitigate the development of adverse events.

In addition to the iNKG2D-U2S3 pairing based upon ULBP2, we have also identified high-affinity orthogonal MicA and ULBP3 variants to iNKG2D.YA that are surprisingly non-redundant in their amino acid compositions through the helix 4 domain (data not shown). The fact that a convergence of sequence was not observed, despite the conserved tertiary structure of the MIC α_1-α_2 domains, indicates that there are many solutions for orthogonality. It will be interesting to see if the helix 4 residues between orthogonal MicA, ULBP3, and ULBP2 variants can be swapped and orthogonality maintained or if there are other ligand-specific residues that contribute to the ability to discriminate between wild-type and iNKG2D.YA. Additionally, we have engineered a completely independent inert NKG2D orthogonal to the above NKG2D.YA and a set of cognate orthogonal ligands by performing mutant ligand screening against the alternative inert variant NKG2D.AF. The iNKG2D.AF inert receptor cannot engage the U2S3 ligand but instead has its own high affinity ULBP2-based ligand, U2R, which in turn, does not bind iNKG2D.YA. This suggests that there is opportunity to explore a breadth of inert NKG2D variants that, in combination with mutational space offered by the varied MIC ligands, will lead to the identification of additional privileged orthogonal receptor-ligand pairings. Having multiple orthogonal inert NKG2D receptors and respective cognate orthogonal ligand pairs provide many potential applications including designing CAR constructs based on mutually exclusive receptor-ligand

---

[75] Paulina J. Paszkiewicz et al., "Targeted Antibody-Mediated Depletion of Murine CD19 CAR T Cells Permanently Reverses B Cell Aplasia," *The Journal of Clinical Investigation* 126, no. 11 (n.d.): 4262–72, https://doi.org/10.1172/JCI84813.

[76] Brian Philip et al., "A Highly Compact Epitope-Based Marker/Suicide Gene for Easier and Safer T-Cell Therapy," *Blood* 124, no. 8 (August 21, 2014): 1277–87, https://doi.org/10.1182/blood-2014-01-545020.

[77] Xiuli Wang et al., "A Transgene-Encoded Cell Surface Polypeptide for Selection, in Vivo Tracking, and Ablation of Engineered Cells," *Blood* 118, no. 5 (August 4, 2011): 1255–63, https://doi.org/10.1182/blood-2011-02-337360.

[78] Lauren D. Scherer, Malcolm K. Brenner, and Maksim Mamonkin, "Chimeric Antigen Receptors for T-Cell Malignancies," *Frontiers in Oncology* 9 (March 5, 2019), https://doi.org/10.3389/fonc.2019.00126.

[79] Alec J. Walker et al., "Tumor Antigen and Receptor Densities Regulate Efficacy of a Chimeric Antigen Receptor Targeting Anaplastic Lymphoma Kinase," *Molecular Therapy: The Journal of the American Society of Gene Therapy* 25, no. 9 (06 2017): 2189–2201, https://doi.org/10.1016/j.ymthe.2017.06.008.

pairs. For example, one might introduce them into different cell populations, such as CD4 and CD8 T-cells, to differentially engage them as needed with a fusion to the appropriate orthogonal ligand. Furthermore, within the same cell, the two iNKG2D variants could be expressed, engineered such that the activation signal is split into distinct sets of intracellular signaling domains. Engagement of one inert CAR with a tumor-targeting MicAbody be insufficient to drive effective cytolysis but engagement of the second inert CAR with a its own cognate, distinct tumor-targeting MicAbody would result in the collaboration or complementation of signaling events to promote T cell function, thereby requiring dual antigen recognition to discriminate between natural and transformed cells. Alternatively, engagement of the first inert CAR via its cognate MicAbody targeting a tumor antigen could activate the T cell while a MicAbody directed at a target that is present on healthy cells could generate a secondary, immunosuppressive signal to the CAR-T cell via the other cognate inert CAR that would enhance the discriminatory power of the T cells.

The antibody-based format of MicAbodies provides significant advantages that include the incorporation of Fv portions of clinically approved or late-stage development antibodies, relative ease of manufacturing and purification with transient transfection yields comparable to those of the parental antibodies (data not shown), and a favorable PK profile that will translate into a convenient frequency of administration to patients. For all of the antigen targets that we have thus far explored with the *convertible*CAR system, the light-chain fusion of U2S3 compares favorably with the heavy-chain format in directing cytolytic activity (data not shown). However, in the instances where a difference in cytolytic efficiency was observed, the light-chain fusion resulted in greater target cell killing. This is exemplified in the case of the rituximab-MicAbody where U2S3 fusion to the light-chain of the antibody resulted in better outcomes *in vitro* and *in vivo*. Other adaptor-based systems have also observed that the location of ligand fusion on the targeting domain can play a significant role in directing CAR-T cell activity as it defines the functional distance between effector and target cells which can vary between different antigenic targets and even different epitopes on the same target[80]. It appears that fusion to the light-chain may play a similar role in situations where epitope location may confine the functional proximity of *convertible*CAR-T cells to the target cell.

In summary, the *convertible*CAR-T system is a universal chimeric antigen receptor platform that has demonstrated capabilities to not only be readily targeted to different antigens but can also be selectively engaged exogenously to drive cell expansion. The privileged receptor-ligand interaction that has been developed is agnostic to cell type and can, in principle, be engineered into any cell of interest as long as the appropriate signaling domains are provided. Additionally, the adoptive cellular therapy field is aggressively pursuing the development of allogeneic effector cells [81] [82] to bring down the cost of

[80] Rodgers et al., "Switch-Mediated Activation and Retargeting of CAR-T Cells for B-Cell Malignancies."
[81] Hiroki Torikai and Laurence Jn Cooper, "Translational Implications for Off-the-Shelf Immune Cells Expressing Chimeric Antigen Receptors," *Molecular Therapy: The Journal of the American Society of Gene Therapy* 24, no. 7 (2016): 1178–86, https://doi.org/10.1038/mt.2016.106.
[82] Marco Ruella and Saad S. Kenderian, "Next-Generation Chimeric Antigen Receptor T-Cell Therapy: Going off the Shelf," *BioDrugs: Clinical Immunotherapeutics, Biopharmaceuticals and Gene Therapy* 31, no. 6 (December 2017): 473–81, https://doi.org/10.1007/s40259-017-0247-0.

therapy and provide a more consistent, readily accessible product[83] [84] [85]. A powerful synergistic effort would be to implement a universal CAR system, the modularity of which is defined by extracellular engagement of the *convertible*CARs, thus translating polyfunctionality[87] [86] into fewer iterations of effector cell re-engineering. Once a truly universal allogeneic CAR system has been validated, the therapeutic field then becomes characterized by the relative ease of developing and implementing a library of adaptor molecules from which selections can be made based upon the indication being addressed. This also broadens the potential areas of application to any pathogenic cell, including those cells that are chronically infected or provoking autoimmunity, provided that there is present an accessible targetable surface antigen.

---

[83] Sophie Viaud et al., "Switchable Control over in Vivo CAR T Expansion, B Cell Depletion, and Induction of Memory," *Proceedings of the National Academy of Sciences of the United States of America* 115, no. 46 (13 2018): E10898–906, https://doi.org/10.1073/pnas.1810060115.

[84] Fraietta et al., "Determinants of Response and Resistance to CD19 Chimeric Antigen Receptor (CAR) T Cell Therapy of Chronic Lymphocytic Leukemia."

[85] D. Sommermeyer et al., "Chimeric Antigen Receptor-Modified T Cells Derived from Defined $CD8^+$ and $CD4^+$ Subsets Confer Superior Antitumor Reactivity *in Vivo*," *Leukemia* 30, no. 2 (February 2016): 492–500, https://doi.org/10.1038/leu.2015.247.

[86] John Rossi et al., "Preinfusion Polyfunctional Anti-CD19 Chimeric Antigen Receptor T Cells Are Associated with Clinical Outcomes in NHL," *Blood* 132, no. 8 (August 23, 2018): 804–14, https://doi.org/10.1182/blood-2018-01-828343.

FIGURES

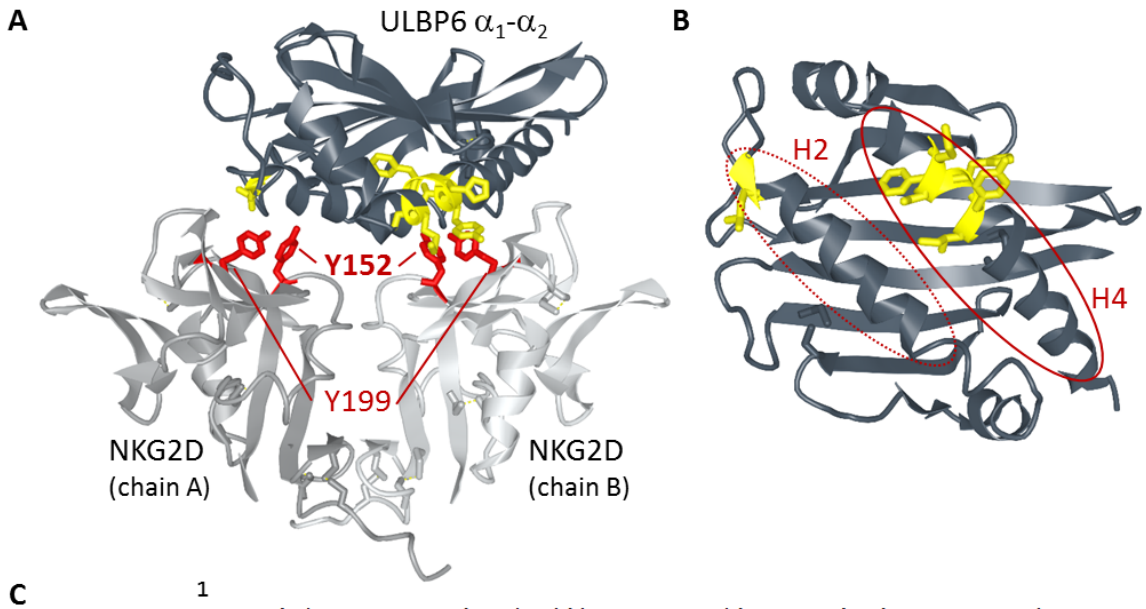

C

```
            1
ULBP6       RRDDPHSLCYDITVIPKFRPGPRWCAVQGQVDEKTFLHYDCGNKTVTPVSPLGKKLNVTMAWKAQ
ULBP2       GRADPHSLCYDITVIPKFRPGPRWCAVQGQVDEKTFLHYDCGNKTVTPVSPLGKKLNVTTAWKAQ
U2S3        GRADPHSLCYDITVIPKFRPGPRWCAVQGQVDEKTFLHYDCGNKTVTPVSPLGKKLNVTTAWKAQ
U2R         GRADPHSLCYDITVIPKFRPGPRWCAVQGQVDEKTFLHYDCGNKTVTPVSPLGKKLNVTTAWKAQ

            66              81
ULBP6       NPVLREVVDILTEQLLDIQLENYTPKEPLTLQARMSCEQKAEGHSSGSWQFSIDGQTFLLFDSEK
ULBP2       NPVLREVVDILTEQLRDIQLENYTPKEPLTLQARMSCEQKAEGHSSGSWQFSFDGQIFLLFDSEK
U2S3        NPVLREVVDILTEQLWDIQLENYTPKEPLTLQARMSCEQKAEGHSSGSWQFSFDGQIFLLFDSEK
U2R         NPVLREVVDILTEQLWDIQLENYTPKEPLTLQARMSCEQKAEGHSSGSWQFSFDGQIFLLFDSEK
                   Helix 2

            131                     155
ULBP6       RMWTTVHPGARKMKEKWENDKDVAMSFHYISMGDCIGWLEDFLMGMDSTLEPSAGAP 212
ULBP2       RMWTTVHPGARKMKEKWENDKVVAMSFHYFSMGDCIGWLEDFLMGMDSTLEPSAGAP 212
U2S3        RMWTTVHPGARKMKEKWENDKVVATKLYLWSMGDCIGWLEDFLMGMDSTLEPSAGAP 212
U2R         RMWTTVHPGARKMKEKWENDKVVATLLWGWSMGDCIGWLEDFLMGMDSTLEPSAGAP 212
                                         Helix 4
```

Figure 1: (A) The structure of NKG2D in complex with ULBP6 (Protein Data Bank 4S0U) was used to illustrate the residues in both the NKG2D homodimer and ligand that were targeted for mutagenesis. Light gray chains correspond to the two NKG2D monomers with Tyrosine 152 and Tyrosine 199, important for ligand engagement, highlighted in red. The dark gray chain corresponds to ULBP6 with the locations of residues at 81 and 156-160 that are mutated in the orthogonal ligands are highlighted in yellow. PDB files were manipulated in NCBI's iCn3D 3D Structure Viewer (https://www.ncbi.nlm.nih.gov/Structure/icn3d/full.html) **(B)** The ULBP6 same structure but with NKG2D absent and the ligand rotated 90° to reveal the two critical helix domains – H2 and H4 - that engage with the NKG2D homodimer. **(C)** The ULBP2 and ULBP6 α_1-α_2 domains are 96.7% identical with the only alignment differences in red font, the locations of helices 2 and 4 underlined, the NNK library residues highlighted in gray, and the residues incorporated into the final orthogonal ligands - ULBP2.S3 (U2S3) and ULBP2.R (U2R) for iNKG2D.YA and iNKG2D.AF, respectively - indicated in blue. Numbering is based upon the mature protein.

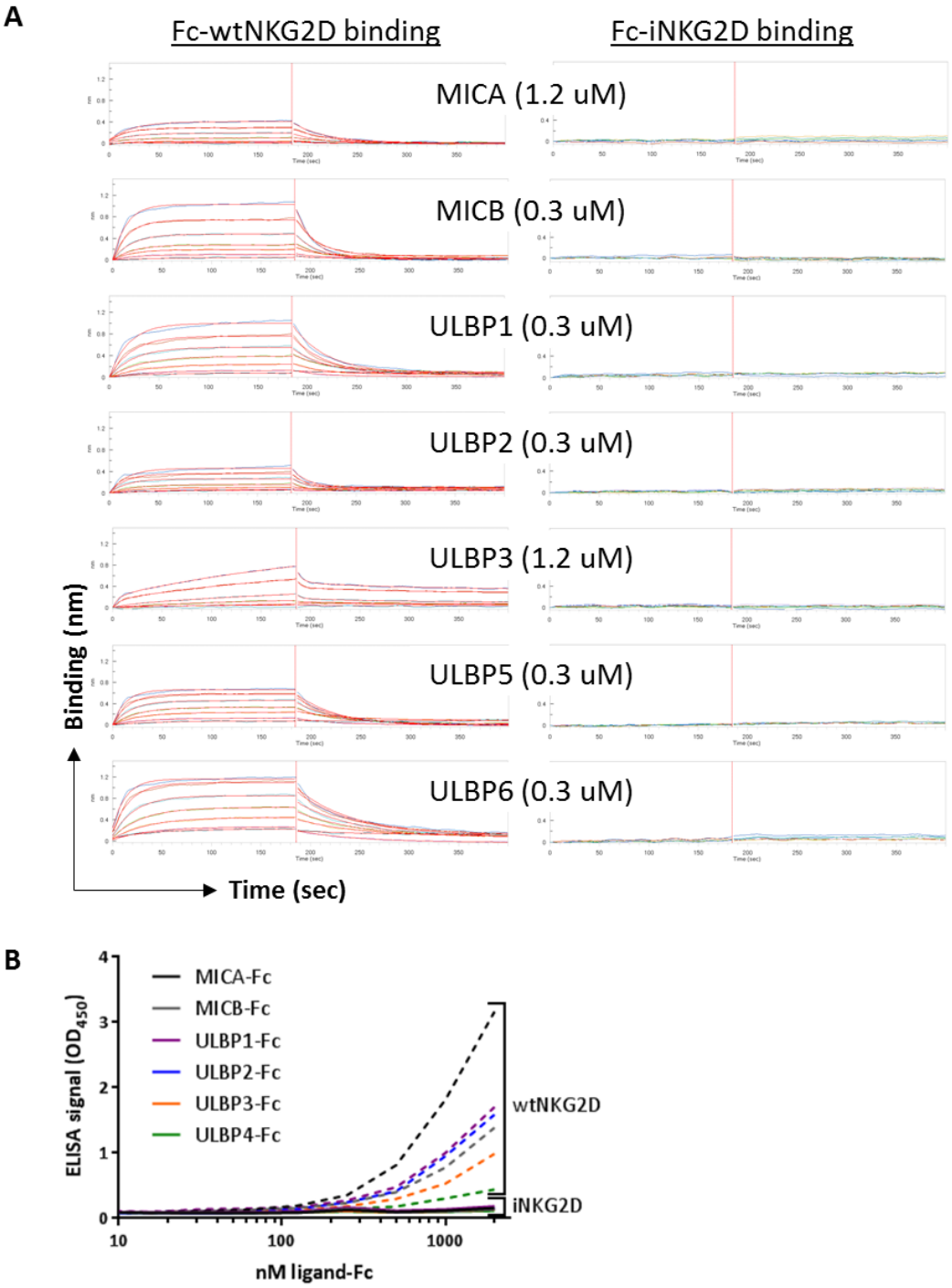

Figure 2: (A) Octet BLI kinetic binding data for His-tagged monomeric wild-type MIC ligand interaction with either wild-type NKG2D or iNKG2D. Fc-wtNKG2D or Fc-iNKG2D.YA were captured with anti-human IgG Fc capture (AHC) biosensor tips associated with a dilution series of each ligand (parenthetical value indicates highest concentration examined) after baseline establishment. ULBP4 could not be expressed and purified as a monomer so was not included in this assay. Note that all axes are to the same scale. **(B)** ELISA confirming inability of iNKG2D.YA to engage natural ligands. Ligand-Fc fusions (R&D Biosystems) were coated onto microtiter plates and a titration of biotinylated Fc-NKG2D (dashed lines) or Fc-iNKG2D.YA (solid lines) applied and detected by streptavidin-HRP.

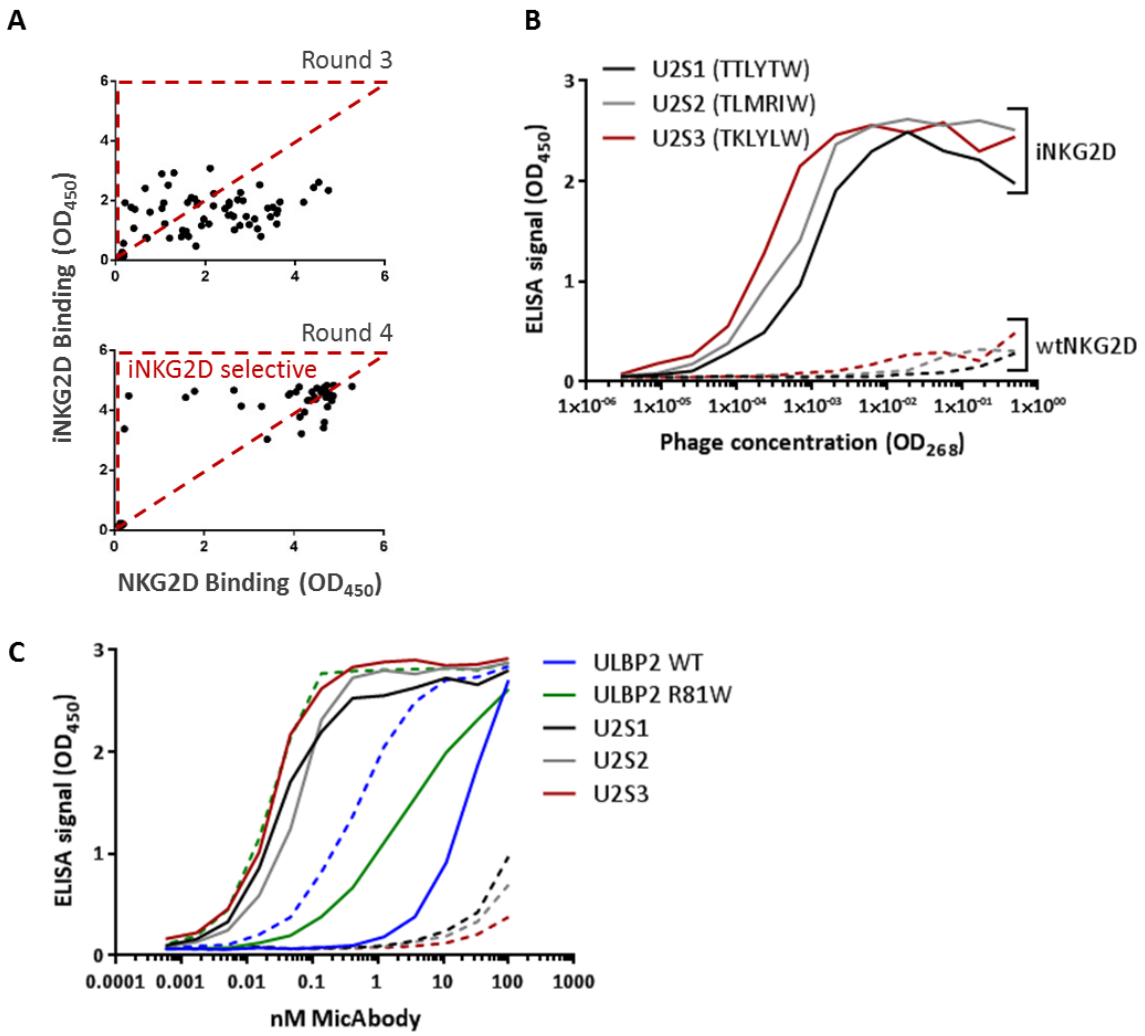

Figure 3: (A) Relative binding of selected phage to Fc-iNKG2D.YA and Fc-wtNKG2D after the third and fourth rounds of panning in the presence of increasing concentrations of wtNKG2D competitor. Phage clones in the upper left portion of the graph outlined by the red triangle were selected for further characterization. **(B)** Three phage clones – S1, S2, S3 – were amplified and after phage particle normalization tested for their ability to selectively engage plate-bound Fc-iNKG2D.YA (solid lines) over Fc-wtNKG2D (dashed lines) in an ELISA. Sequences in the helix 4 region are parenthetically indicated and all clones additionally have an R81W mutation. **(C)** All three variants along with wild-type ULBP2 and ULBP2 with the R81W mutation were expressed as fusions to the C-terminus of the anti-FGFR3 antibody clone R3Mab heavy chain and purified MicAbodies were tested for the ability of the selective ULBP2 variants to retain preferential Fc-iNKG2D.YA binding (solid lines) over Fc-wtNKG2D (dashed lines). All purified MicAbodies retained binding to human FGFR3 (data not shown).

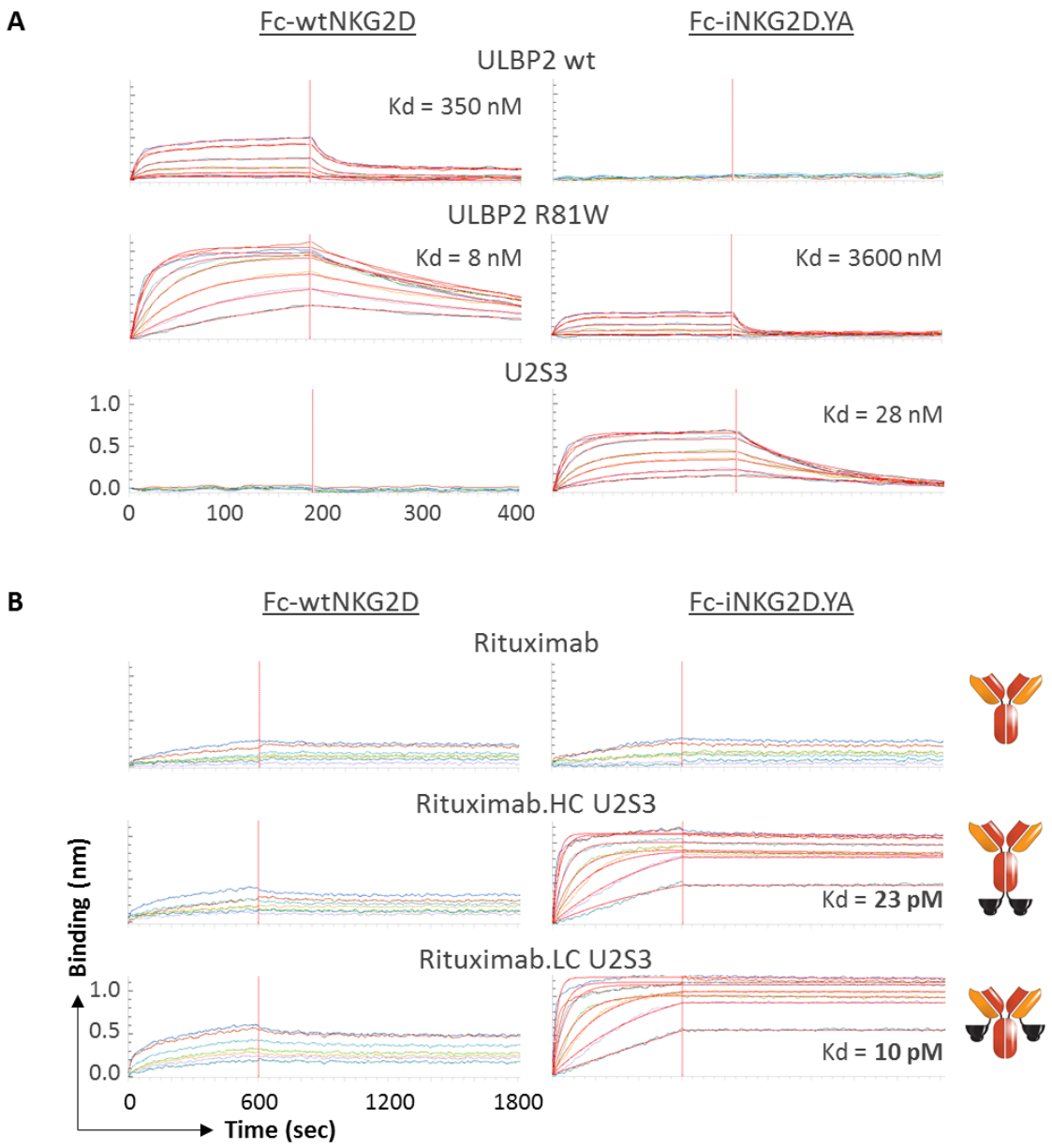

Figure 4: (A) Binding analysis of His-tagged monomeric wild-type ULBP2, ULBP2 R81W, and the orthogonal U2S3 ligand binding to Fc-NKG2D and Fc-iNKG2D.YA. Experimental set-up as described in Figure 2. **(B)** Verification that U2S3 orthogonality is maintained when it is fused to the C-terminus of either the heavy or light chain of rituximab. Fc-NKG2D or Fc-iNKG2D.YA were captured on anti-human IgG Fc biosensor tips and baseline established before exposed to the bispecific MicAbodies. The y-axes corresponding to binding responses were set to the same scale for all sensograms.

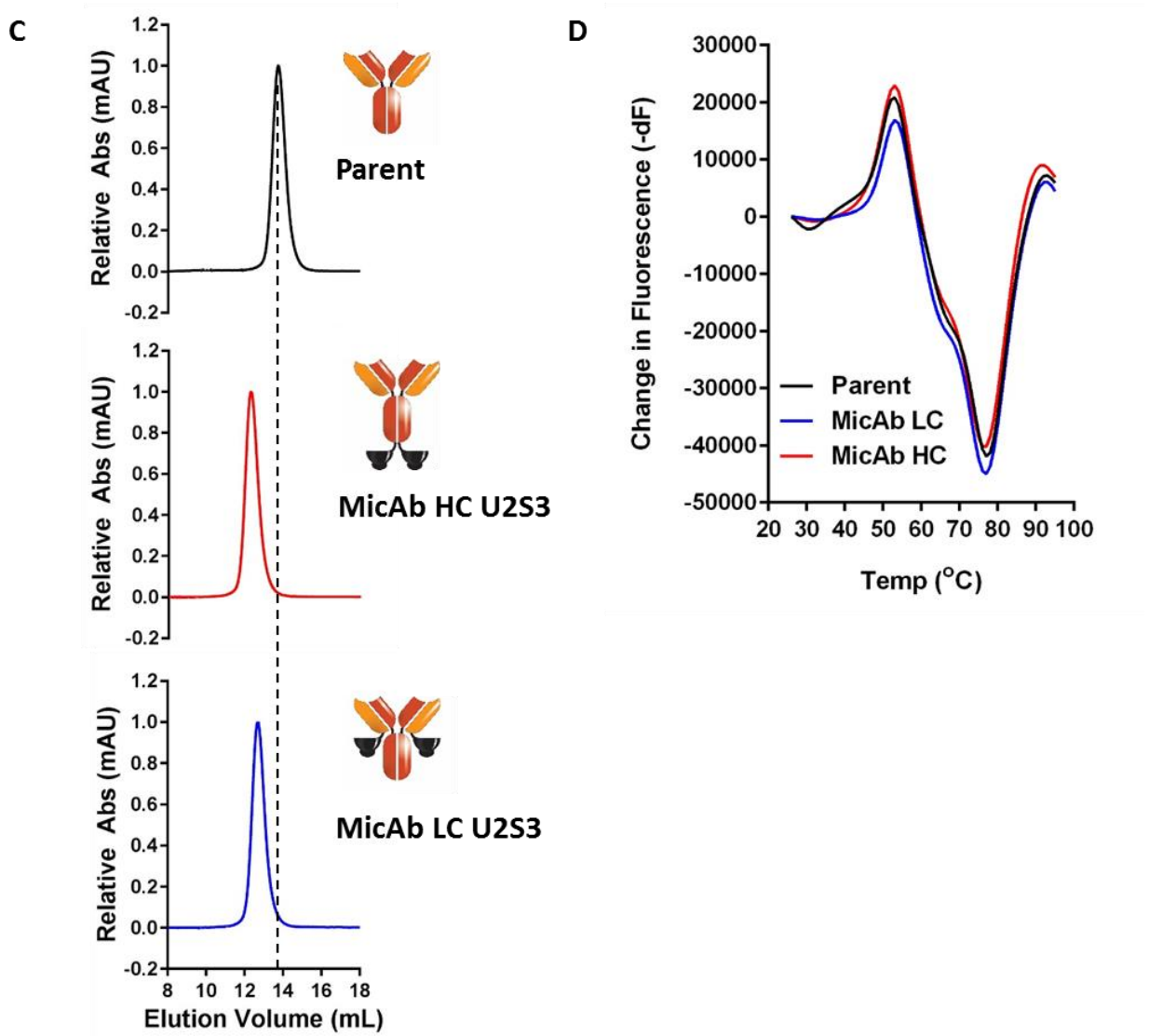

Figure 4 - continued: (C) SEC profiles of Rituximab-based MicAbodies after fractionation. **(D)** Thermostability characterization of parent (ADCC-) and both heavy- and light-chain fusions of Rituximab-U2S3. Equal amounts of protein were subject to a +1°C/minute melting curve in the presence of SYPRO Orange, changes in fluorescence quantified in a StepOnePlus™ Real-Time PCR System, and fluorescence profiles overlayed.

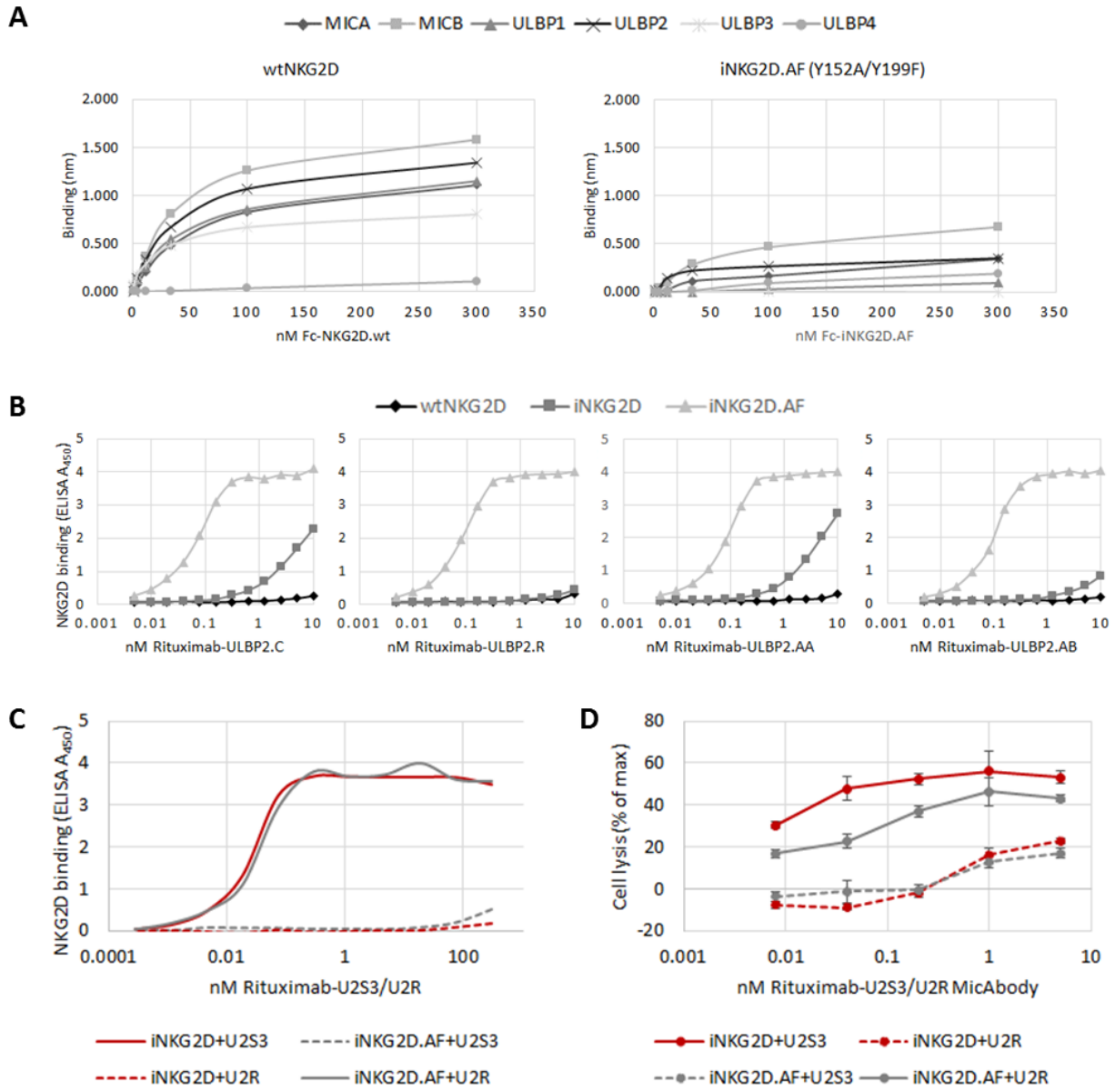

Figure 5: Orthogonal ULBP2 ligand selective binding to NKG2D Y152A/199F (iNKG2D.AF). Library design and phage panning performed as described for iNKG2D.YA except that biotinylated double-mutant Fc-iNKG2D.AF was used during rounds of selection against increasing concentrations of Fc-wtNKG2D competitor. **(A)** Octet BLI binding data for interaction of monomeric ligands to either Fc-wtNKG2D or Fc-iNKG2D.AF. **(B)** Lead variants selected from the phage display library were cloned as fusions to the C-terminus of the Rituximab light chain and differential binding to Fc-wtNKG2D, Fc-iNKG2D.YA, and Fc-iNKG2D.AF and quantified by ELISA. Shown are four variants that selectively engage Fc-iNKG2D.YA and not the other two receptors. **(C)** ELISA demonstrating exclusivity of U2S3 and U2R ligand binding to the receptor variant against which it was selected – Fc-iNKG2D.YA and Fc-iNKG2D.AF, respectively. **(D)** Calcein release assay with Ramos target cells at an E:T of 20:1 with either iNKG2D.YA-CAR or iNKG2D.AF-CAR expressing CD8+ T cells and a titration of Rituximab.LC-U2S3 or Rituximab.LC-U2R.

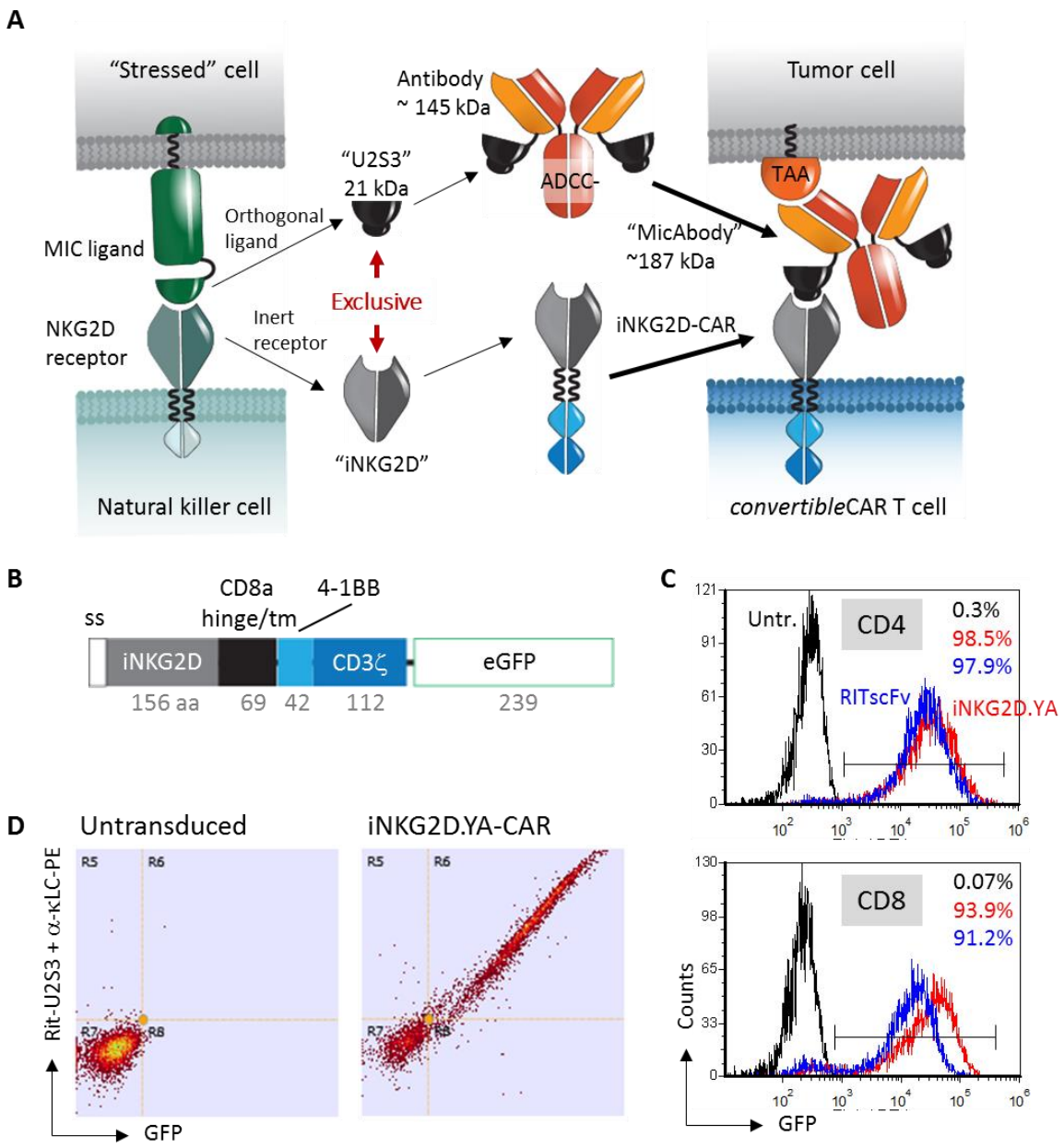

Figure 6: (A) Overview of engineering steps to convert the components of the NKG2D-MIC axis into an orthogonal and privileged interaction. iNKG2D.YA and U2S3 became the components of a second generation CAR receptor and bispecific adaptor molecule (MicAbody), respectively. **(B)** Structure of the iNKG2D-CAR construct encompassing the costimulatory 4-1BB domain in addition to CD3zeta and fused at the C-terminus to EGFP. **(C)** Example of high efficiency lentiviral transduction of the iNKG2D.YA-CAR into either CD4 or CD8 cells without sorting for GFP positive events. The RITscFv-CAR has the same structure as the iNKG2D-CAR except that the scFv based upon the VH/VL domains of rituximab was used instead of iNKG2D. **(D)** Surface expression of iNKG2D.YA was determined in CD8+ T cells by incubating cells with Rituximab.LC-U2S3 MicAbody followed by PE-conjugated mouse-anti-human kappa chain antibody staining. Data were plotted to directly compare GFP with MicAbody staining

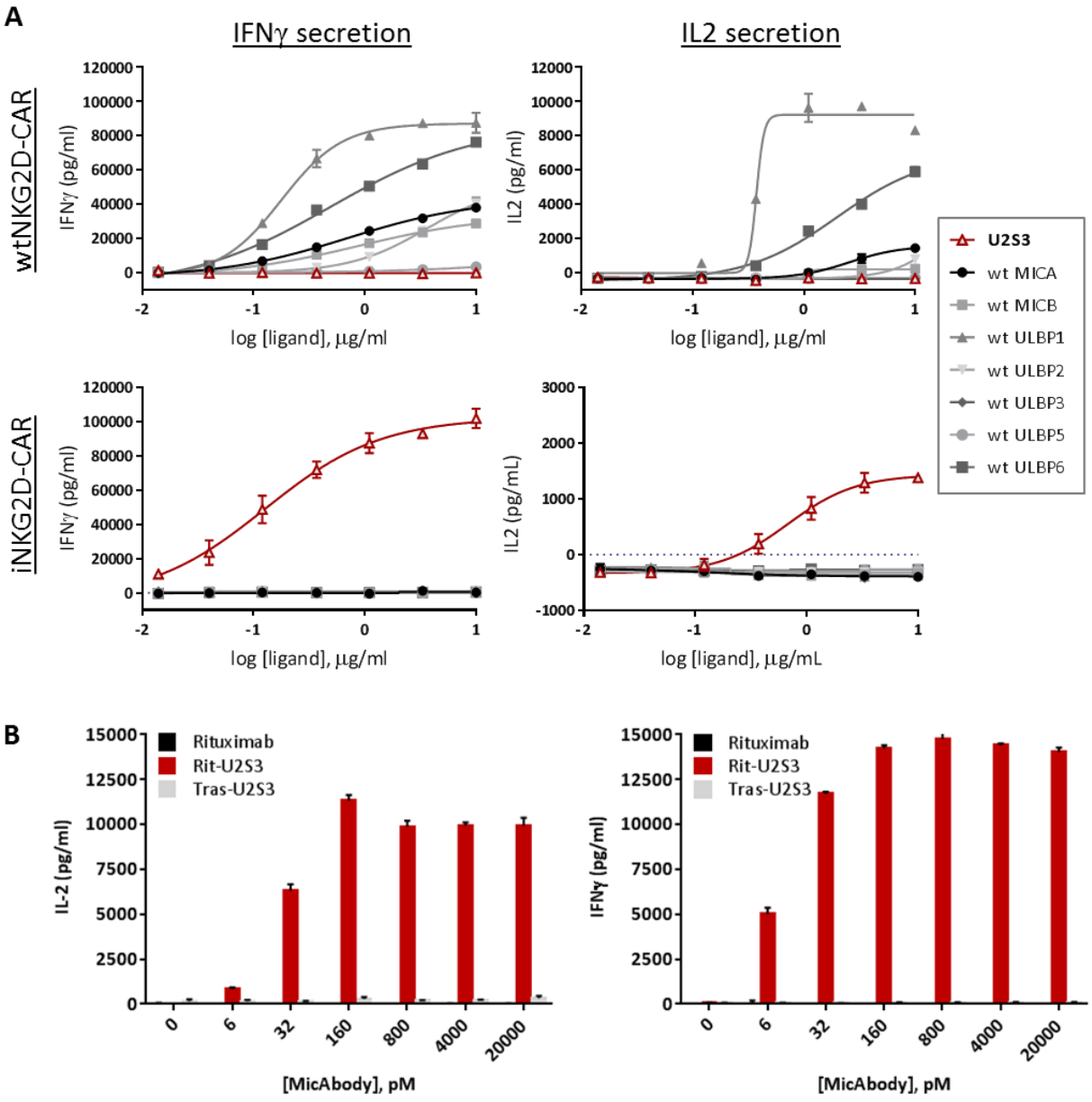

Figure 7: Ligand-dependent activation of iNKG2D-CAR expressing $CD8^+$ T cells. **(A)** CD8+ T cells were transduced with CAR constructs comprised of either wild-type NKG2D or iNKG2D.YA as the receptor domain. Wild-type His-tagged monomeric ligands or His-tagged monomeric U2S3 were coated onto the wells of a microtiter plate in a 1:3 dilution series starting at 10 ug/mL. $1x10^5$ CAR expressing cells were introduced to the wells in 150 uL volume without exogenous IL2, supernatants collected 24 hours later, and the amount of cytokine produced and release quantified by cytokine-specific ELISA. ULBP4 was not included in the assay as a His-tagged version could not be expressed and purified. **(B)** Ramos (CD20+) target cells were exposed to iNKG2D.YA-CAR CD8+ cells at an E:T of 5:1 in the presence of increasing concentrations of Rituximab antibody (without U2S3 ligand), Rituximab.LC-U2S3 MicAbody, or Trastuzumab.LC-U2S3 MicAbody. After 24 hours, supernatants were harvested and IL-2 (left panel) or IFNγ (right panel) quantified by ELISA.

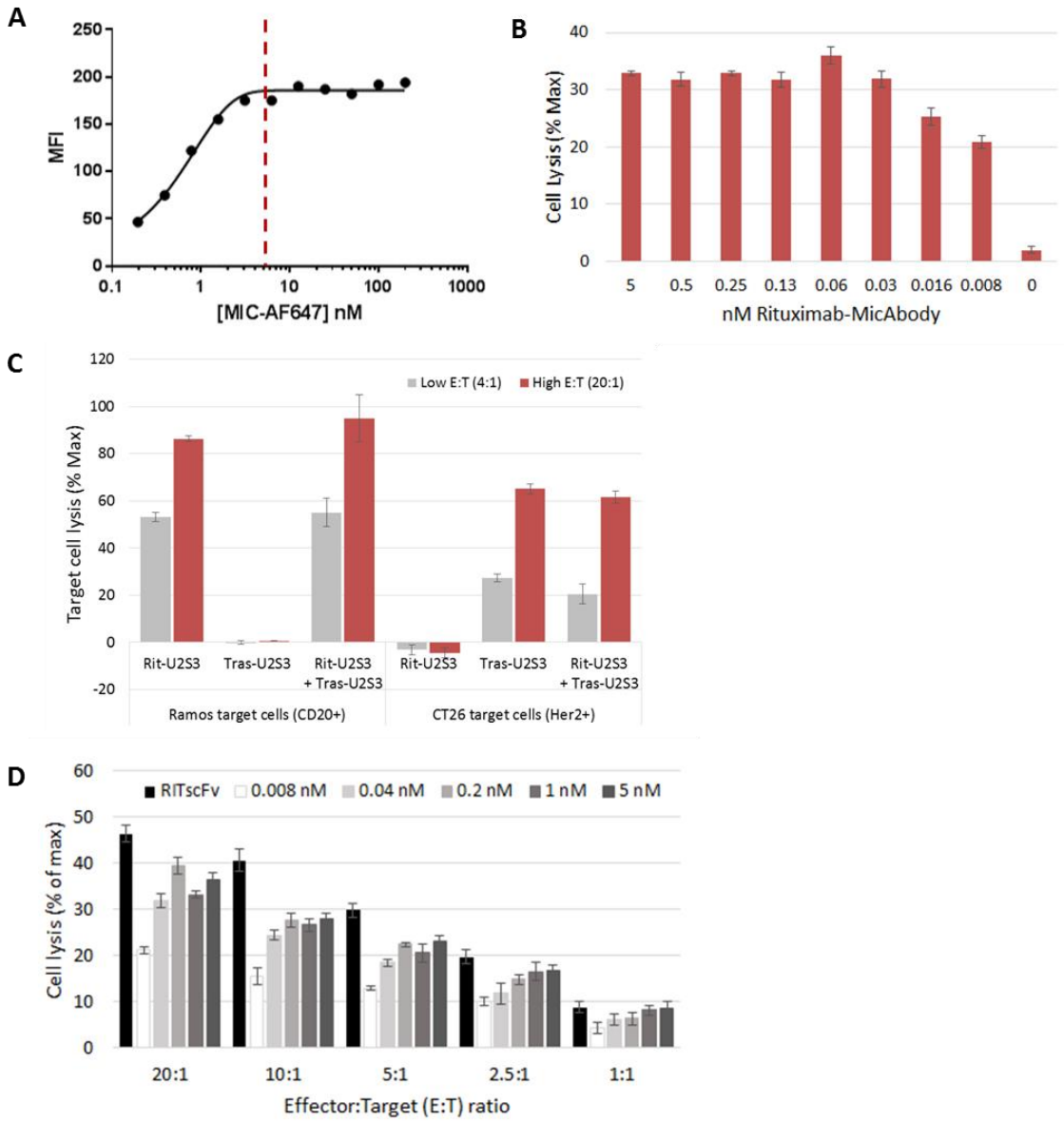

Figure 8: *In vitro* characterization of iNKG2D-CAR activity. **(A)** iNKG2D.YA-CAR CD8+ cells were incubated with increasing concentrations of Alexa Fluor 647 conjugated Rituximab.LC-U2S3 for 30 minutes, the excess washed away, and the MFI quantified by flow cytometry to ascertain the concentration at which maximal MicAbody association occurs. **(B)** iNKG2D.YA-CAR CD8+ cells were armed with increasing concentrations of Rituximab.LC-U2S3 as described in (A) then co-incubated with calcein-loaded Ramos cells at an E:T of 10:1 for two hours after which the amount of released calcein was quantified. **(C)** To demonstrate multiplexing capabilities, iNKG2D-CAR CD8+ cells were pre-armed with 5 nM Rituximab.LC-U2S3, 5 nM Trastuzumab.LC-U2S3, or an equimolar mixture of 2.5 nM of each (5 nM total) as described in (B) then exposed to calcein-loaded Ramos or CT26-Her2 cells at two indicated E:T ratios. The amount of calcein released was quantified after two hours. Error bars reflect standard deviation for replicates in the assay. **(D)** Lysis of Ramos target cells at different E:T ratios of a RITscFv-CAR or iNKG2D.YA-CAR, the latter for which Rituximab.LC-U2S3 MicAbody was also titrated for each E:T. Liberated calcein was quantified after two hours.

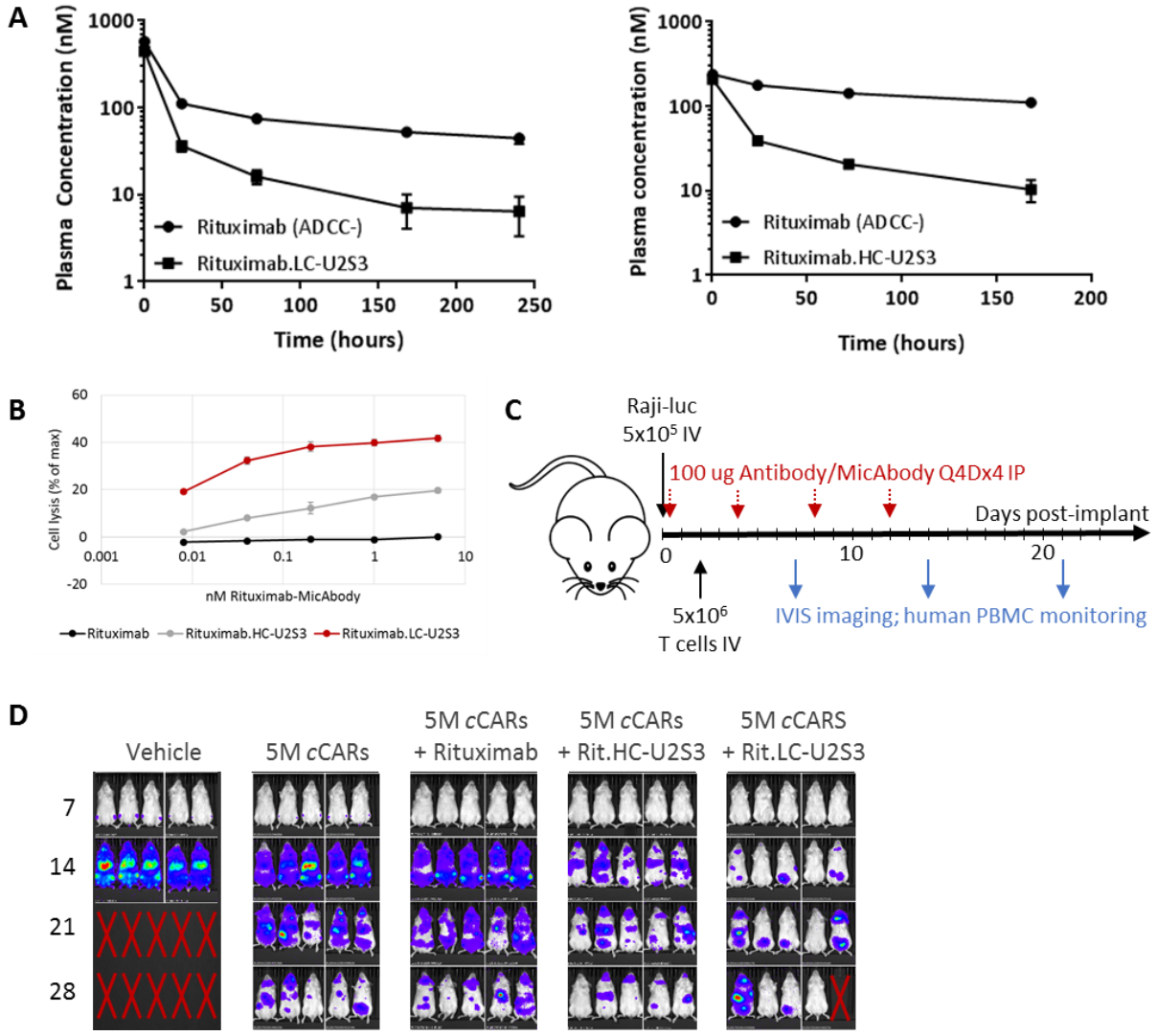

Figure 9: Comparison of heavy- vs. light-chain U2S3 fusions to Rituximab (ADCC-) antibody. **(A)** Pharmacokinetics of serum Rituximab-U2S3 MicAbody levels after 100 ug IV administration in NSG mice in the absence of human T cells or tumor. Note that all MicAbodies and antibody controls used were ADCC-deficient. The graph on the left is a comparison of parental antibody to the light-chain U2S3 fusion while the graph on the right is a comparison of parental antibody to the heavy-chain U2S3 fusion. **(B)** *In vitro* calcein release assay after two hours co-culture with iNKG2D-CAR CD8+ T cells and Ramos target cells at an E:T of 20:1 and titrations of Rituximab-MicAbodies. Error bars represent ±SD for the experiment and data are representative of multiple experiments. **(C)** *In vivo* study design in NSG mice with Raji-luciferase cells invused IV followed by treatment and monitoring as indicated. CD4 and CD8 cells were independently transduced, combined at a 1:1 ratio without adjusting for percent transduction, and a total of $5x10^6$ *convertible*CAR-T cells (*c*CARs) were injected IV. **(D)** IVIS imaging was performed 7, 14, 21, and 28 days post-implantation and all adjusted to the same scale. Death of mouse #5 at day 28 of the 5M iNKG2D + Rituximab.LC-U2S3 was unrelated to treatment or disease. All others indicated deaths were due to disease.

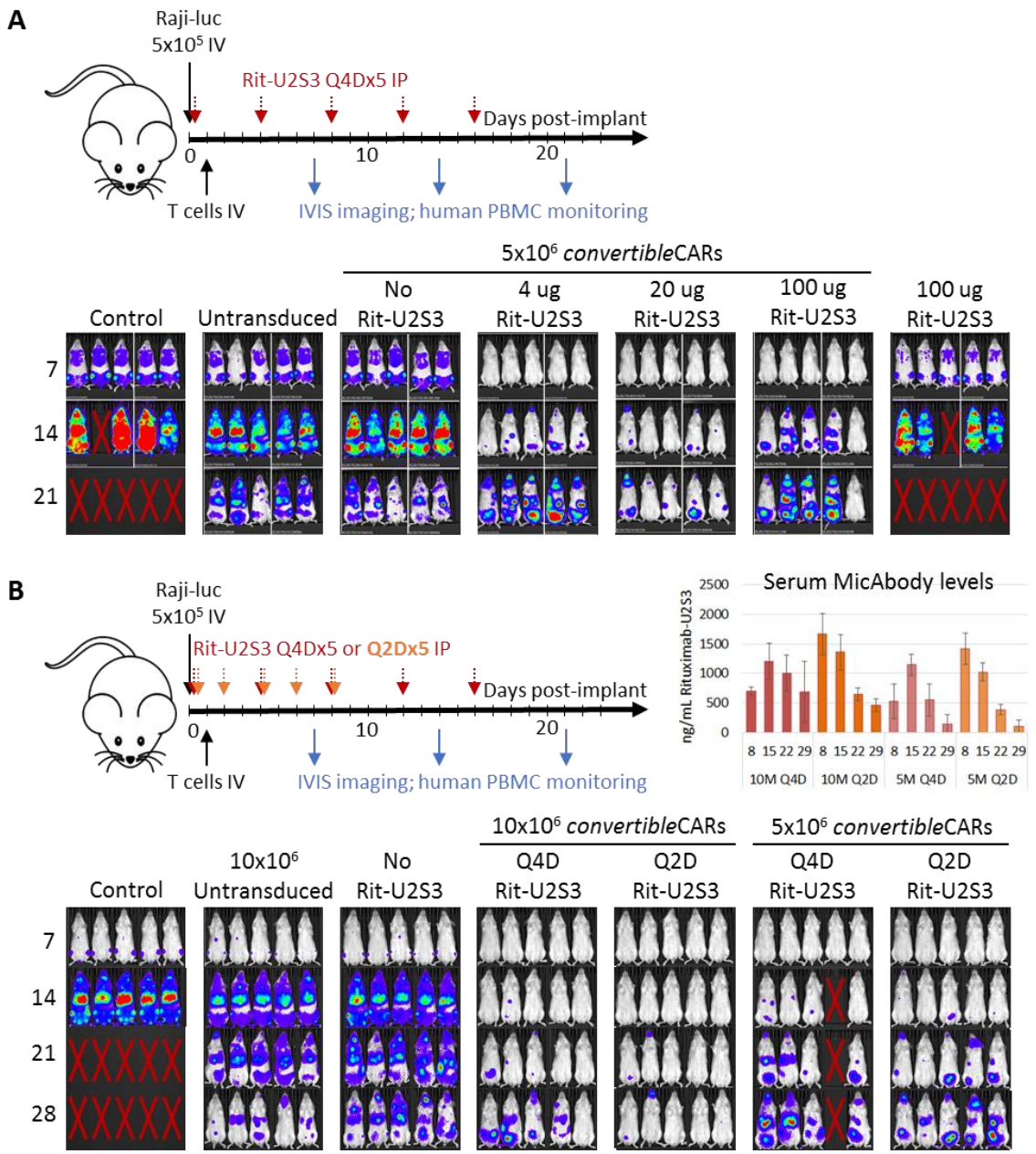

Figure 10: Investigation of both MicAbody and *convertible*CAR dosing strategy in a disseminated Raji-luciferase B cell lymphoma NSG mouse model. **(A)** Rituximab.LC-U2S3 Q4Dx5 dosing was initiated the same day as tumor implantation at 4, 20, or 100 ug per dose while keeping the number of cells administered constant across cohorts. The 100 ug Rituximab.LC-U2S3 only cohort – without any CAR-T cells – received just a single dose of MicAbody. **(B)** Frequency of MicAbody dosing as well as *convertible*CAR-T cell infusions levels were explored with the former being administered either every two or four days for a total of 5 doses, and the latter at either $5x10^6$ or $10x10^6$ total cells infused. Mouse #4 in the Q4D + $5x10^6$ cohort that died by day 14 did so for reasons unrelated to treatment or disease. Serum levels of Rituximab.LC-U2S3 were also monitored at 8, 15, 22, and 29 days post-implantation for all cohorts that received MicAbody (cohorts that did not receive any were negative by ELISA, data not shown). IVIS images within each respective study were adjusted to the same scale.

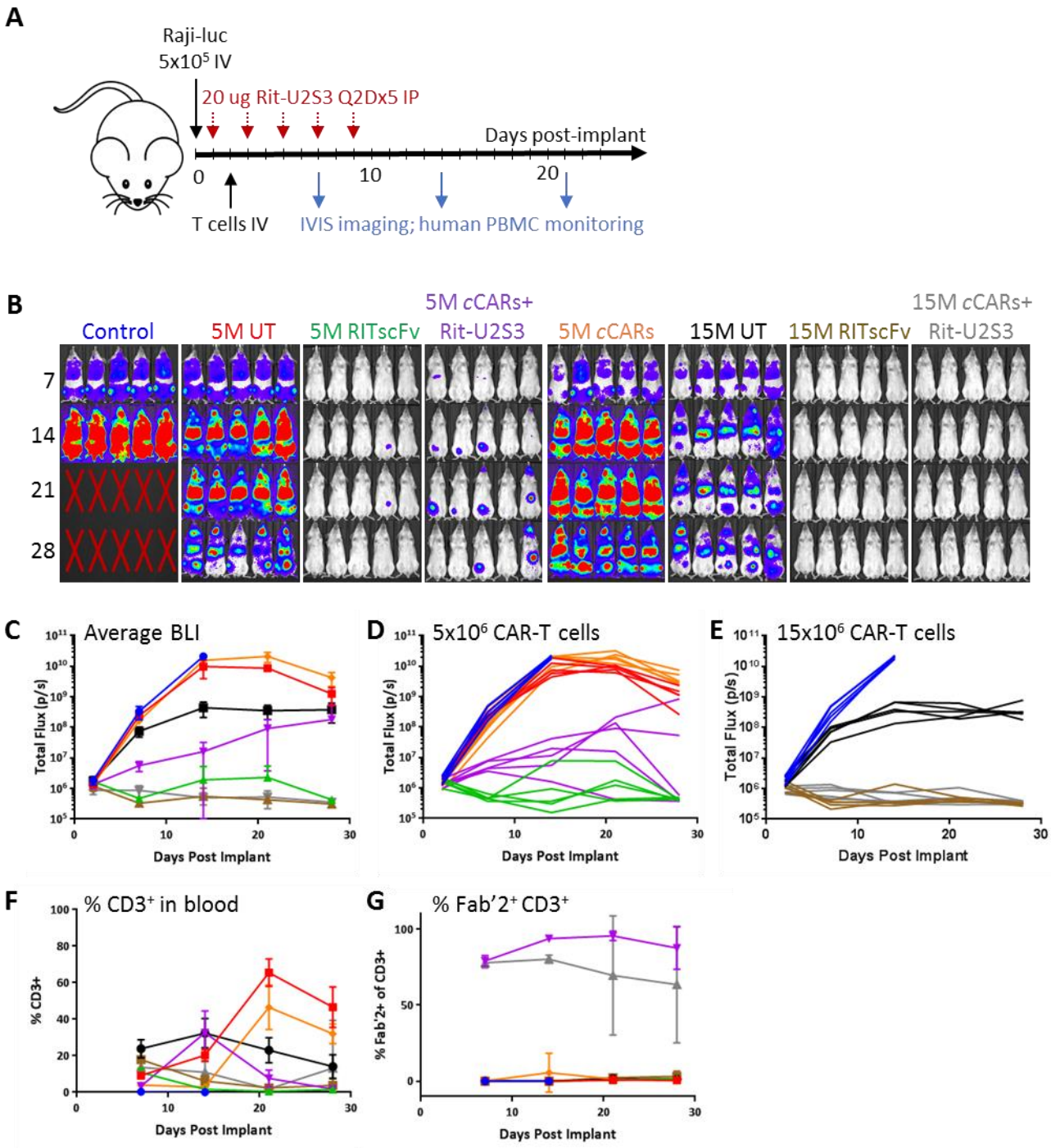

Figure 11: Control of a disseminated Raji B cell lymphoma in NSG mice. **(A)** Study design in NSG mice with Raji-luciferase cells implanted IV followed by treatment and monitoring as indicated. **(B)** IVIS imaging was performed 7, 14, 21, and 28 days post-implantation and all adjusted to the same scale. **(C)** Average luminescent output ±SD for each cohort along with individual animal traces for the groups that received **(D)** $5x10^6$ or **(E)** $15x10^6$ total T cells. T cell dynamics over the course of the study examining **(F)** human CD3+ cells in the blood and **(G)** Bound MicAbody detected by anti-Fab'2. Shown are cohort averages ±SD. Color coding in all graphs matches the labeling on the luminescence images.

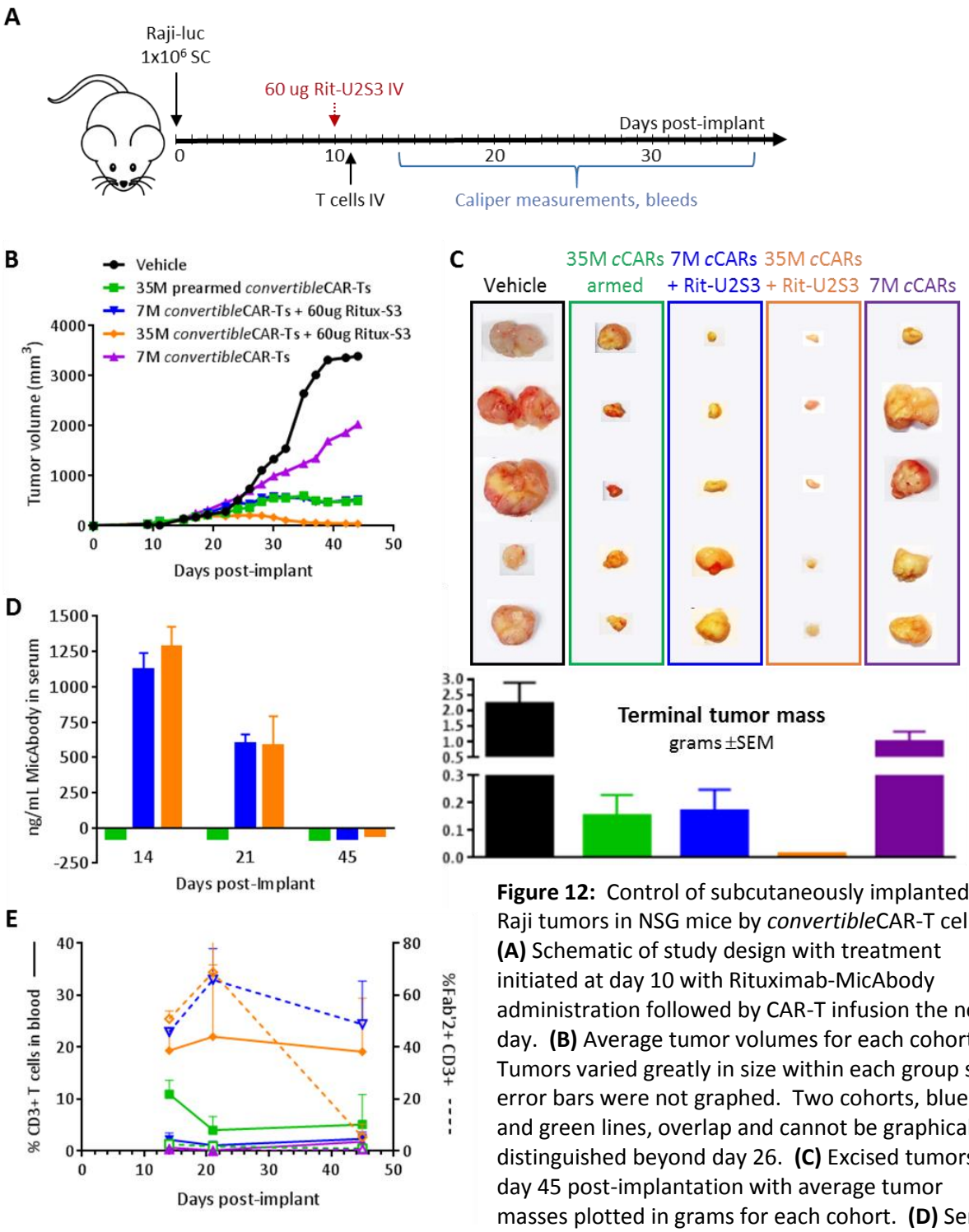

Figure 12: Control of subcutaneously implanted Raji tumors in NSG mice by *convertible*CAR-T cells. **(A)** Schematic of study design with treatment initiated at day 10 with Rituximab-MicAbody administration followed by CAR-T infusion the next day. **(B)** Average tumor volumes for each cohort. Tumors varied greatly in size within each group so error bars were not graphed. Two cohorts, blue and green lines, overlap and cannot be graphically distinguished beyond day 26. **(C)** Excised tumors at day 45 post-implantation with average tumor masses plotted in grams for each cohort. **(D)** Serum Rituximab-MicAbody levels. Error bars indicated ±SD. **(E)** CD3+ T cell dynamics in the blood and quantitation of the percentage of T cells with surface-associated MicAbody (Fab'2 staining). Groups are color coded to match across the different graphics.

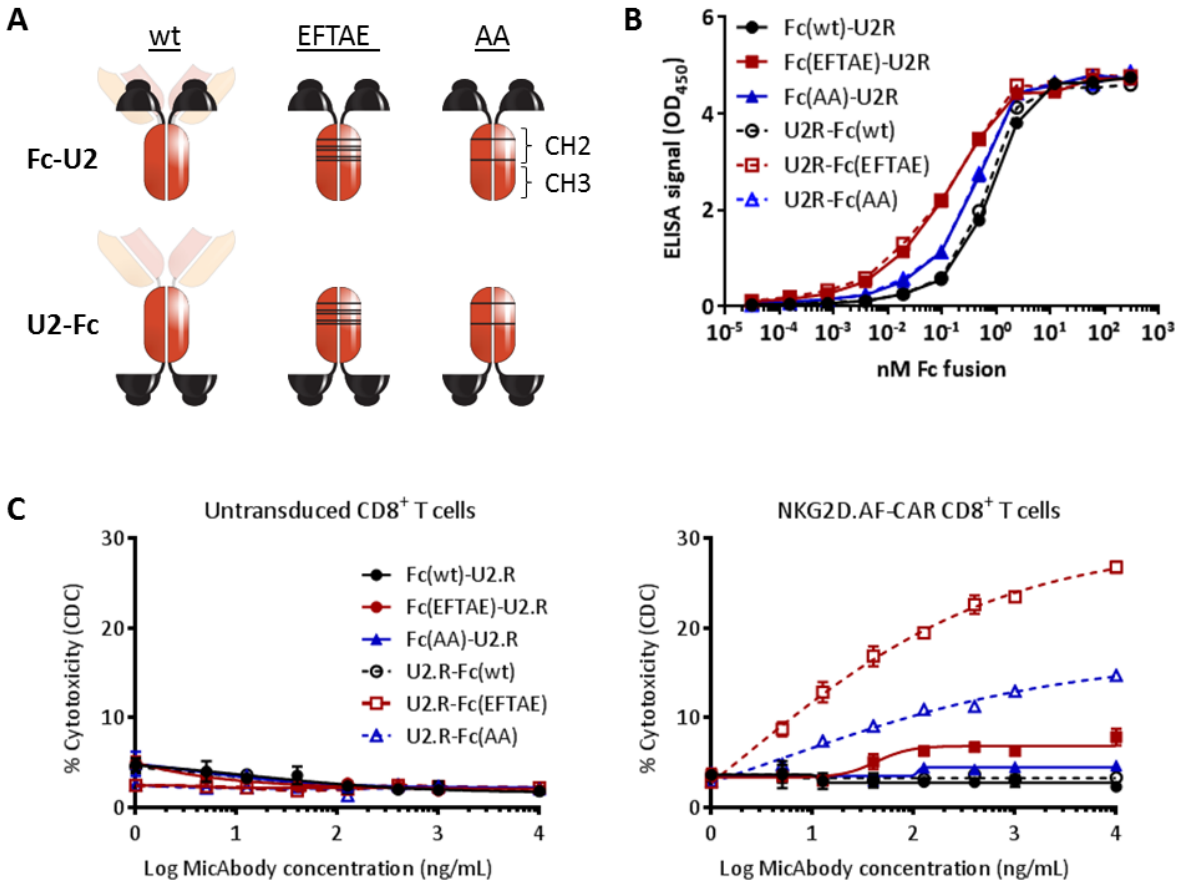

Figure 13: Targeted recruitment of complement factor C1q to NKG2D.AF-CAR cells to direct their complement-mediated attrition. **(A)** Structure of orthogonal ligand fusions to the Fc portion of human IgG expressed as either N- or C-terminal fusions. In addition to wild-type Fc, two sets of mutations in the CH2 domain that enhance C1q binding were independently explored - S267E/H268F/S324T/G236A/I332E (EFTAE) and K326A/E333A (AA). **(B)** ELISA examining binding of human C1q to each purified fusion protein. **(C)** Complement-dependent cytotoxicity (CDC) assays for C1q-binding enhance Fc-fusions. NKG2D.AF-CAR (59% GFP^+) or untransduced CD8+ T cells were incubated with a titration of each fusion molecule and 10% normal human serum complement for three hours before dead T cells were labeled by SYTOX Red and enumerated. Similar results were obtained when the U2S3 orthogonal ligand fusions to direct complement-enhanced Fc domains to iNKG2D-CAR cells (data not shown).

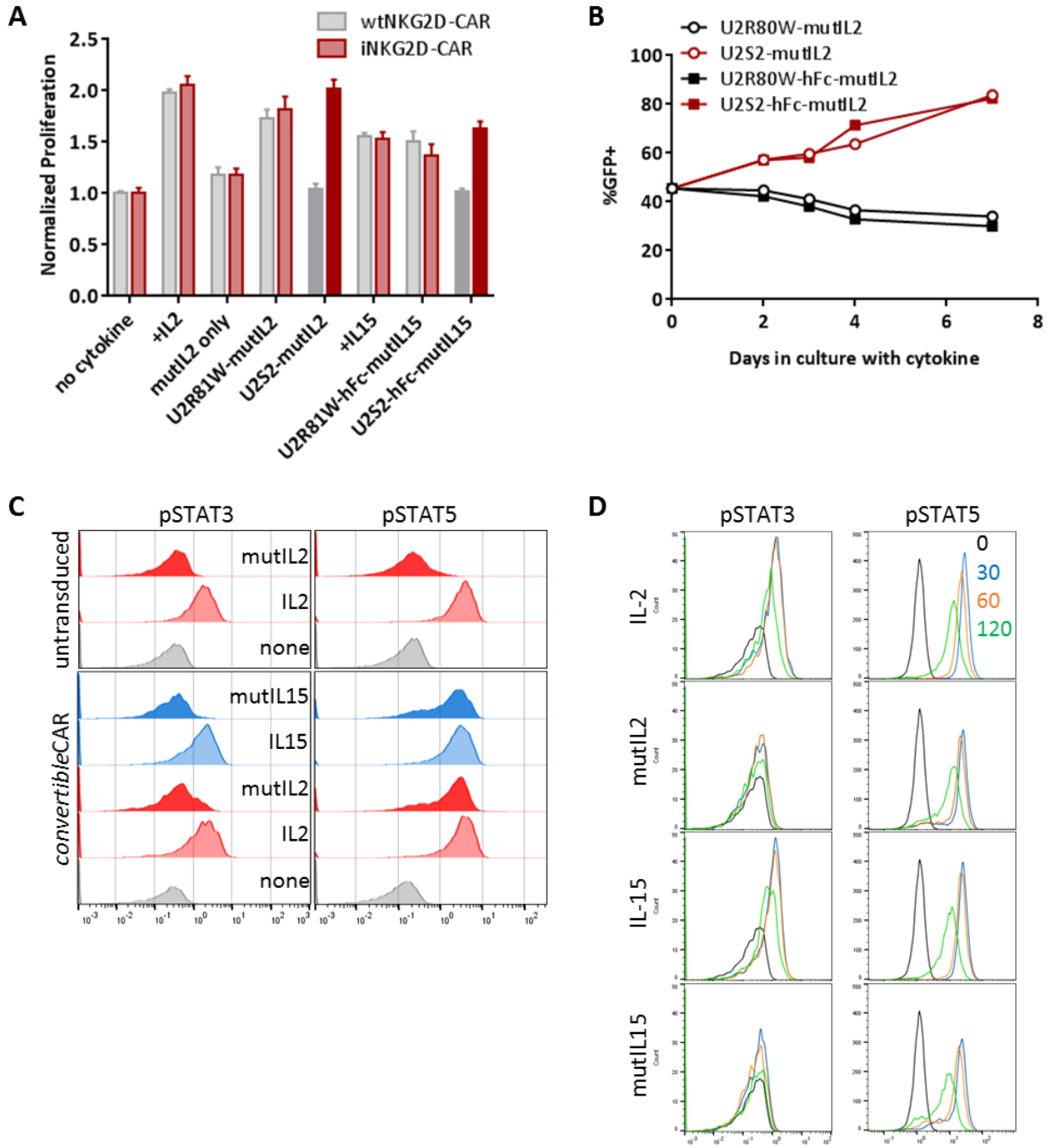

Figure 14: Targeted delivery of mutant-IL2 cytokine to iNKG2D-CAR CD8+ T cells. **(A)** WST *in vitro* proliferation after three days of wtNKG2D-CAR or iNKG2D.YA-CAR (*convertible*CAR) cell treatment with 30 IUe/mL of cytokine or cytokine-U2S2 fusion. Darker shading is to highlight selectivity. **(B)** A low efficiency (45% GFP^+) iNKG2D.YA-CAR transduction was cultured with 30 IUe/mL of non-selective (U2R80W) or iNKG2D.YA-selective (U2S2) mutIL2 fusion and maintained for seven days. Cells were periodically examined by flow cytometry to quantify the $\%GFP^+$ cells in each population. **(C)** Untransduced or *convertible*CAR-CD8 T cells were starved overnight of supporting cytokine then treated with 150 IUe/mL IL-2, IL-15, U2S3-hFc-mutIL2, or U2S3-hFc-mutIL15 for 2 hours before fixing and staining for intracellular phospo-STAT3 and –STAT5. **(D)** *convertible*CAR-CD8 T cells were treated as in (C) except that cells were fixed at 0, 30, 60, and 120 minutes after exposure to cytokines or U2S3-hFc-cytokine fusions then stained for intracellular phospo-STAT3 and –STAT5.

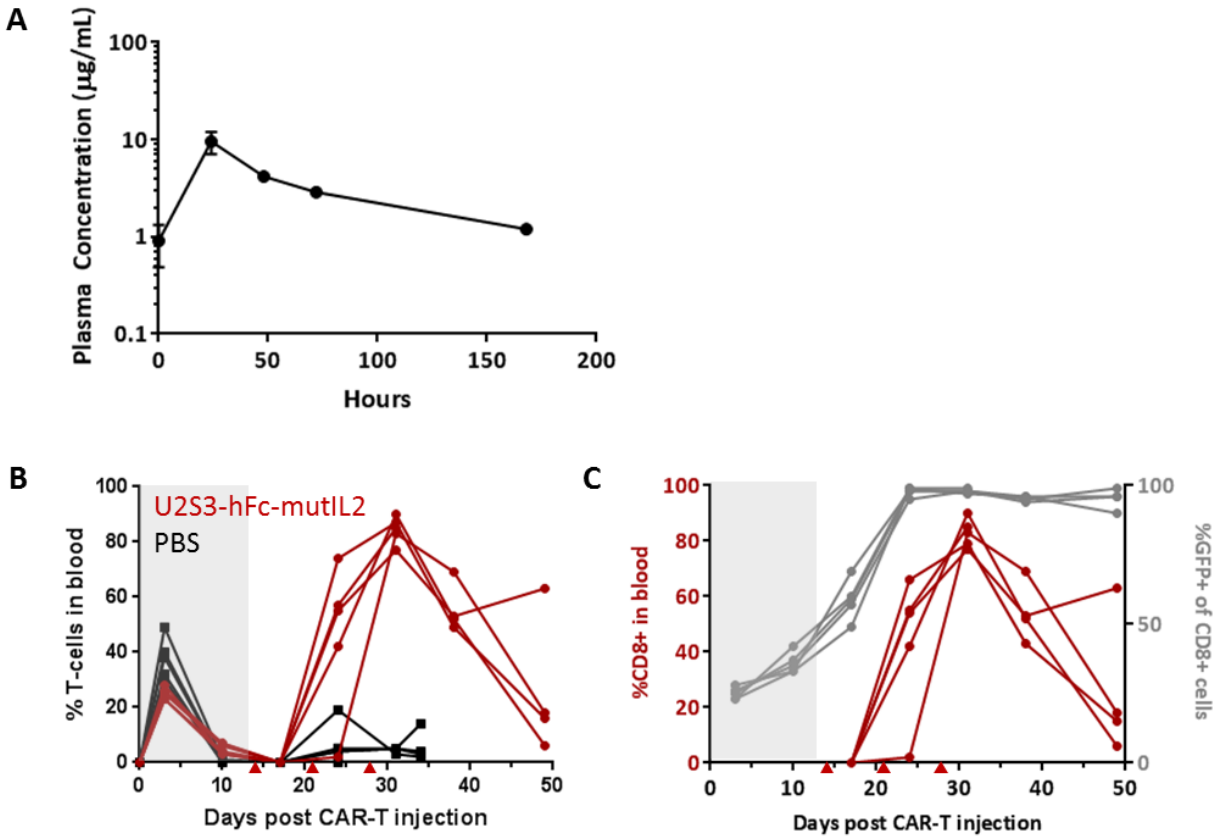

Figure 15: In vivo response of convertibleCAR-T cells to U2S3-hFc-mutIL2. **(A)** Serum PK of U2S3-hFc-mutIL2 after 60 ug IP injection in NSG mice. **(B)** NSG mice were injected with $7x10^6$ total iNKG2D-transduced cells (CD4:CD8 1:1). After contraction of T cells at 14 days, mice were injected with 30 ug U2S3-hFc-mutIL2 or PBS once per week – indicated by red triangles - and T cell dynamics monitored by flow. Shown is the % of human CD3+ T cells in the peripheral blood with each trace corresponding to an individual mouse. **(C)** Plots for the expansion of CD8+ cells as well as the increase in proportion of GFP+ (CAR-expressing) cells upon U2S3-mutIL2 treatment.

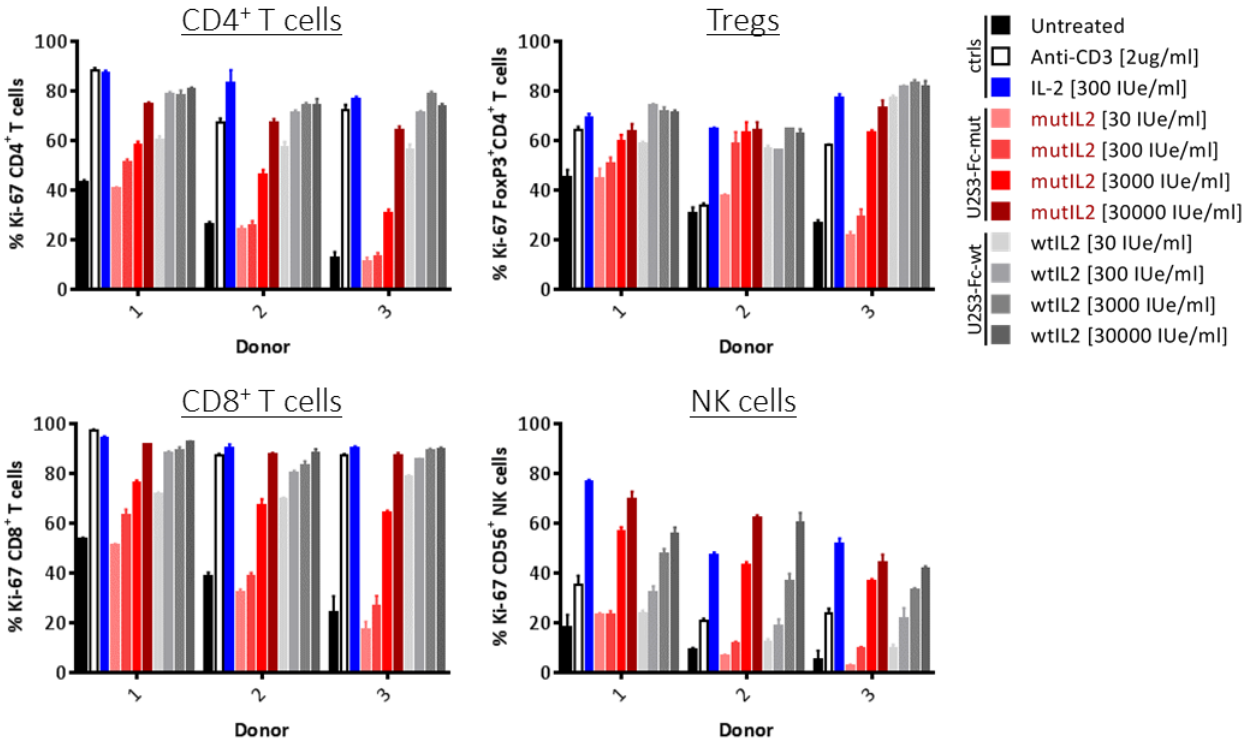

Figure 16: Responsiveness of human PBMCs to U2S3-hFc-mutIL2. Human PBMCs from three donors were incubated with increasing concentrations of U2S3-hFc-mutIL2 or U2S3-hFc-wtIL2 for four days along with controls. Each of the labeled cell types was examined for the marker Ki-67 to quantify proliferative response under each condition. Error bars are ±SD of triplicate measurements.

v. 190708

---------- END OF MANUSCRIPT ----------